American Mineralogist, Volume 96, pages 659–674, 2011

Chromatite and its Cr^{3+}- and Cr^{6+}-bearing precursor minerals from the Nabi Musa Mottled Zone complex, Judean Desert

Ella V. Sokol,[1] Olga L. Gaskova,[1,2] Svetlana N. Kokh,[1] Olga A. Kozmenko,[1] Yuri V. Seryotkin,[1,2] Yevgeny Vapnik,[3,*] and Michail N. Murashko[4]

[1]Sobolev Institute of Geology and Mineralogy, Siberian Branch of Russian Academy of Sciences, 3, Koptug Avenue, Novosibirsk, 630090, Russia
[2]Novosibirsk State University, Pirogova 2, 630090 Novosibirsk, Russia
[3]Department of Geological and Environmental Sciences, Ben-Gurion University of the Negev, P.O.B. 653, Beer-Sheva 84105, Israel
[4]Systematic Mineralogy, 44, 11th line V.O, apt. 76, Saint-Petersburg 199178, Russia

Abstract

Chromatite ($CaCrO_4$, tetragonal) is mainly known from Cr^{6+}-contaminated soils associated with chromium ore processing residue. This extremely rare mineral was found at the Nabi Musa locality (Judean Desert, Israel), in a peculiar rock complex of the Mottled Zone. We have explored the possible mechanisms responsible for leaching Cr^{6+} from natural rocks, by means of field observations, batch experiments, thermodynamic modeling, and mineralogical analyses of the Nabi Musa rocks (XRPD, EMPA, SEM, FTIR, and optical microscopy). A remarkable feature of the Mottled Zone rocks is a broad occurrence of high- and ultrahigh-temperature combustion metamorphic rocks, with Cr^{3+} accumulated mainly in opaque minerals such as Fe-spinel, brownmillerite, and perovskite. Another feature of the Mottled Zone sequence is abundant Cr^{3+} (bentorite and volkonskoite) and Cr^{6+} mineralization (Cr^{6+}-bearing ettringite and baryte-hashemite solid solution) in low-temperature hydrothermal veins. Field, mineralogical, and thermodynamic modeling data suggest that Cr was leached from Cr^{3+}-bearing opaque minerals during late hydrothermal alteration of combustion metamorphic rocks by unusual hyperalkaline waters (pH up to 12). The Cr^{3+} was then oxidized to Cr^{6+}, and subsequently partially immobilized in Cr^{6+}-bearing ettringite. As a consequence of the highway construction across Nabi Musa hill in 2006, the buried veins filled by Cr^{6+}-substituted ettringite were exhumed and exposed to supergene alteration. The ensuing decomposition of Cr^{6+}-bearing ettringite was followed by Cr^{6+} release into pore waters in rainy seasons, and then by precipitation of chromatite on the evaporation barrier under the hard desert insolation in dry seasons. The chromatite formation has been due to both unique rock and water chemistry of the Mottled Zone sequence and to the arid climate of the Judean Desert.

Keywords: Chromatite, calcium chromate dehydrate, hexavalent chromium mineralization, Cr^{6+}-bearing ettringite, bentorite, hyperalkaline waters, Mottled Zone, Judean Desert

Introduction

Chromium is present in soils, minerals, and rocks mainly as Cr^{3+}, whereas Cr^{6+} compounds form and very rarely remain stable under natural, near-surface conditions. Chromium can enter the environment through several natural processes, such as weathering, volcanic exhalation, or biogeochemical processes, as well as through human activities. Hexavalent Cr is relatively mobile in supergene environments. It is commonly leached by rain and thaw water from dumps and then migrates into soils and into surficial and ground waters. Reactions of Cr^{6+}-bearing solutions with soil mineral matter produce cryptocrystalline solid precipitates (chromatite, crocoite, and baryte-hashemite solid solutions) in the vicinity of Cr-bearing waste repositories (Palmer 2000; Bajda 2005). Unlike the manmade precipitates, natural chromatite ($CaCrO_4$, tetragonal system, space group $I4_1/amd$) is a very rare mineral. Until recently, it was reported from a single locality of the Maale Adummim complex in the so-called Mottled Zone (MZ), the Judean Desert (Eckhardt and Heimbach 1963; Gross 1977).

We discuss data from another chromatite locality, newly discovered in the Mottled Zone: Nabi Musa hill 5 km southeast of the Maale Adummim area (Fig. 1). Our research has focused on gaining precise information about Cr^{3+}- and Cr^{6+}-bearing minerals in the MZ complex. We attempt to infer the Cr sources and chromatite origin from the available field and analytical evidence (assemblages, chemistry, and morphology of the minerals), coupled with thermodynamic modeling.

The Mottled Zone

Geology and mineralogy

There are 15 complexes composed of peculiar rocks known as the Mottled Zone, or the Hatrurim Formation, on both sides of the Dead Sea Transform, in Israel and Jordan, within Upper Cretaceous marine, calcareous sediments (Fig. 1). The Mottled Zone (MZ) is a melange of diverse sediments (indurated chalk-like mass, marl, limestone, less abundant dolomite, chert, and phosphorite) with numerous foci of high-temperature, low-pressure combustion metamorphic (CM) rocks. All strata are densely veined and altered by late hydrothermal solutions

* E-mail: vapnik@bgu.ac.il

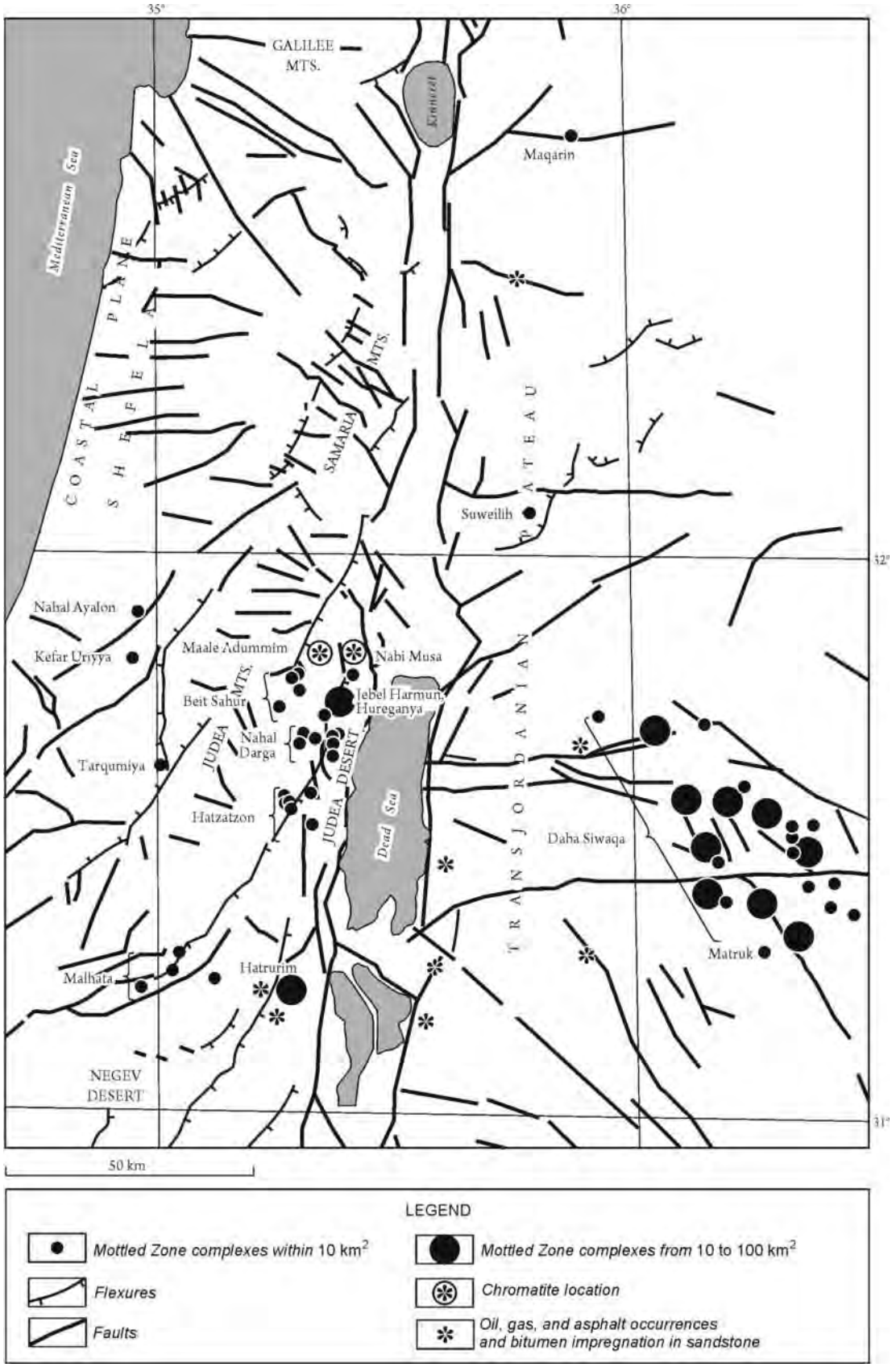

FIGURE 1. Generalized geology of the Dead Sea Transform area (modified after Sokol et al. 2010), with locations of outcrops of the Mottled Zone sequence in Israel and Jordan, as well as hydrocarbon seeps.

(Picard 1931; Bentor et al. 1963; Gross 1977; Burg et al. 1999; Sokol et al. 2010).

There has been much controversy about the origin of the MZ complexes. The best grounded hypotheses invoked diagenesis (Picard 1931), in situ oxidation and combustion of Senonian bituminous chalks with mean C_{org} contents of 8–12 wt% (Bentor et al. 1963), or hydroexplosions and hydrothermal alteration (Gilat 1998), but no study could definitely account for all their structural, mineralogical, and geochemical features. New geological, chemical, and petrological data, however, suggest instead, a relation of the MZ complexes to Pliocene-Quaternary mud volcanism (Vapnik et al. 2007; Sokol et al. 2010), with the heat required for combustion metamorphism probably maintained from burning methane.

Several types of high-temperature combustion metamorphic rocks in the Mottled Zone form numerous separate outcrops, mainly composed of Ca-rich, Al-depleted, and silica-undersaturated spurrite marble and larnite rock. Calcination of calcareous and marly sedimentary parent rocks with low aluminosilicate content under high (750–1000 °C) or ultrahigh (1200–1500 °C) temperatures and ambient pressure lead to the formation of various anhydrous Ca-Al-(Fe)-oxides and Ca-silicates that are typical of both sanidinite facies (Gross 1977; Matthews and Gross 1980; Vapnik et al. 2007; Sharygin et al. 2008; Sokol et al. 2010) and Portland cement clinker (Gross 1977; Kolodny 1979; Clark et al. 1994; Alexander and Smellie 1998).

Unlike most CM complexes worldwide (Grapes 2006; Sokol and Volkova 2007), those in the MZ underwent deep retrograde, hydrothermal alteration and were converted into the so-called "low-grade Hatrurim" rocks. The retrograde alteration was maintained by an extremely high alkalinity of water, which was inherited by cold water seeps presently in the Jordanian MZ areas (Khoury and Nassir 1982; Clark et al. 1993, 1994; Milodowski et al. 2001; Techer et al. 2006). There are, for instance, hyperalkaline seeps at the Maqarin site that fall into three distinct water composition groups: (1) Ca-OH (pH 12.0 to 12.4), (2) Ca-K-Na-OH-SO_4 (pH > 12.5), and (3) Ca-OH-SO_4 (pH ≤ 12.9).

Prolonged interaction of hyperalkaline waters with rocks within the MZ complexes caused hydration of anhydrous silicates and oxides from the CM rocks and precipitation of tobermorite and other calcium silicate hydrates (CSHs), ettringite, thaumasite, brucite, and portlandite. The very hard, low permeability, fine-grained, low-grade Hatrurim rocks were commonly considered as natural analogs of hydrated Portland cements; the varieties enriched in S in the form of sulfate consist of mineral assemblages similar to those seen as products of calcium sulfoaluminate (CSA) cement hydration, but differ from cement in high carbonation (Gross 1977; Kolodny 1979; Clark et al. 1994; Alexander and Smellie 1998; Milodowski et al. 2001). At some localities, the retrograde rocks are predominant while CM rocks are preserved as dispersed relict varieties. These are, specifically, the localities of Nabi Musa and Maale Adummim north of the Dead Sea (Gross 1977; Gilat 1998; Bogoch et al. 1999; Sokol et al. 2010) (Fig. 1).

The MZ sequence is densely cut by veins that contain calcite, aragonite, ettringite, thaumasite, tobermorites, other CSHs, or rarely opal, vaterite, brucite, and portlandite (Gross 1977; Khoury and Nassir 1982; Techer et al. 2006; Sokol et al. 2010). Besides the crystalline phases, veins in the Maqarin complex bear abundant amorphous CSHs and both calcium aluminosilicate hydrate (CASH) and zeolitic gels (Milodowski et al. 2001).

A key feature of vein mineralization in the MZ complexes is the diversity of both Cr^{3+}- and Cr^{6+}-bearing minerals (Fig. 2) (Gross 1977, 1980; Khoury and Nassir 1982; Techer et al. 2006; Elie et al. 2007). We discovered Cr^{6+}-bearing ettringite and chromatite in outcrops of the Nabi Musa area (31°48′N, 35°25′E) in

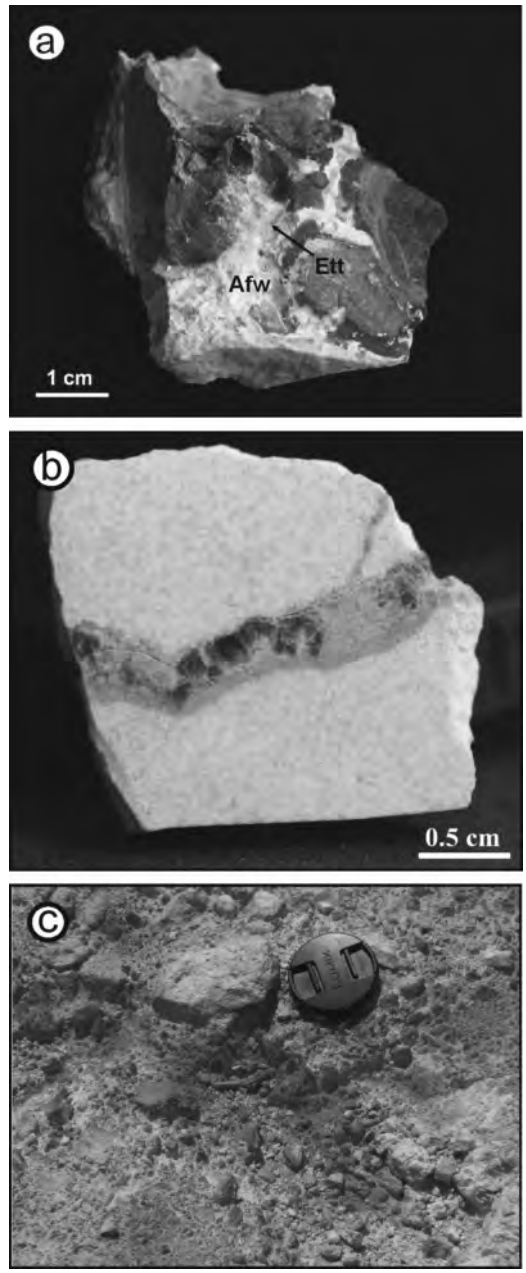

Figure 2. (**a**) Typical Cr^{6+}-bearing ettringite and afwillite filling a crack in a combustion metamorphic rock. The brown color is due to abundant Cr^{3+}-bearing brownmillerite, Fe-spinel, and Ca ferrite. Sample Ettr-5, Maale Adummim MZ area, 2010. (**b**) Bentorite vein in low-grade Hatrurim rock. Hatrurim Basin MZ area, 2010. (**c**) Field occurrence of chromatite precipitates on the surface of $CaCO_3$- and gypsum-cemented low-grade Hatrurim rocks, at the foot of Nabi Musa hill, May 2007; the lens cap is 6 cm in diameter. Abbreviations: Ett = ettringite, Afw = afwillite.

the Judean Desert (Fig. 1). Nabi Musa is a typical MZ complex, existing as a double-crested hill covering an area of 0.46 km^2. It became familiar to geologists from the report of Picard (1931), but it was not until the construction of the Jerusalem-Jericho highway across the hill in 2006 that a complete section of the MZ sequence was exposed. For details of local geology and characteristics of rocks of the Nabi Musa MZ complex, see Sokol et al. (2010). In the field trip of 2005–2007, we failed to find chromatite at the neighboring Maale Adummim locality (31°49′N, 35°22′E), where it was discovered in 1963 (Eckhardt and Heimbach 1963), but we saw numerous small veins with segregations of Cr-bearing ettringite.

Table 1. Major (wt%) and trace element (ppm) composition of Maastrichtian bituminous chalk and Campanian phosphorites

	Maastrichtian bituminous chalk			Campanian phosphorites	
	n	average	st.dev.	average *n* = 185	st.dev.
SiO_2	377	9.30	2.9	3.07	3.81
TiO_2	169	0.16	0.08	0.04	0.02
Al_2O_3	377	3.80	1.8	0.47	0.45
Fe_2O_3	387	1.70	0.78	0.35	0.40
MgO	246	0.94	0.67	0.56	0.78
CaO	302	34.20	3.8	50.9	2.89
Na_2O	95	0.24	0.11	0.56	0.26
K_2O	88	0.34	0.06	0.07	0.05
P_2O_5	241	2.70	1.6	25.7	4.71
SO_3	293	6.80	1.8	2.44	1.33
Org. C	387	10.30	3.0	0.7	1.17
CO_2	134	25.40	3.7	11.4	4.93
Cl	–	–	–	0.53	0.76
F	–	–	–	3.0	0.5
Total	–	95.88	–	99.89	–
Sr	115	1082	196	2300	564
Ba	123	88	55	338	318
Cr	127	285	48	227	75
Ni	126	150	33	89	29
Mn	127	40	18	40	25
V	122	86	19	155	78
Zn	126	251	70	521	204
Mo	127	18.4	7	41	19
U	–	–	–	111	49
Cu	127	94	21	29	20

Notes: The data on the Maastrichtian bituminous chalk bulk composition from Yoffe et al. (2002); minor and trace elements from Minster et al. (1996); data on phosphorites from Nathan et al. (1979) and Gill (1995). *n* = number of samples. st.dev. = standard deviation.

Chromium source rocks

Chromium, as well as Zn, Cu, Ni, Mo, U, and V are trace elements that precipitate in suboxic and fully anoxic bottom-water environments and accumulate in marine sediments, such as oil shale (Cr up to 200–1000 ppm) and phosphorite (Cr up to 1500–7000 ppm) (Piper 1994, 2001; Piper and Calvert 2009). These sediments are abundant in the Levant area, (Eastern Mediterranean, exactly where all known MZ complexes are located), which is an integrated result of Late Campanian–Early Maastrichtian phosphogenesis and oil shale accumulation in highly bioproductive basins (Abed et al. 2005). The Maastrichtian organic-rich ("bituminous") pelagic sediments have been traditionally termed "oil shale," though their inorganic fraction is largely dominated by calcite (Yoffe et al. 2002). Average concentrations of metals in this "oil shale" are (in parts per million) Cr = 256, Ni = 136, Zn =271, Cu = 83, V = 78, and as low as 31 ppm Mn. Chromium contents are typically 100–400 ppm in the phosphorite of the same sedimentary sequence (Table 1), from 100 to 650 ppm in most of the MZ rocks, and as high as a few thousand parts per million in veins rich in Cr-bearing minerals (Bogoch et al. 1999; Elie et al. 2007).

Chromium mineralization in the MZ complexes

Nine Cr-bearing minerals have been found so far in different areas of the MZ. Chromium concentrations are rather high in opaque minerals of combustion metamorphic rocks produced by calcination of the Cr-enriched sedimentary protolith. Cr_2O_3 is the highest (up to 9 wt%) in Fe-spinel and is lower in other opaque phases, which are often rock-forming minerals. It is up to 4.3 wt% in brownmillerite, 3.4 wt% in perovskite, and 1.1 wt% in hematite. Among the studied silicates, the highest Cr_2O_3 (9.7 wt%) was determined in Ti-rich andradite from paralavas (Sharygin et al. 2008; Sokol et al. 2010).

Volkonskoite, commonly accompanied by amorphous Cr^{3+} oxide and hydroxides, is widespread among low-grade Hatrurim rocks, especially in veins at the base of the MZ sequence within the Hatrurim, Nahal Darga, and Nahal Ayalon sites in Israel, as well as in the Daba-Siwaqa and Khyshaym Matruk complexes in Jordan. In addition to volkonskoite, the veins are filled with calcite and minor amounts of gypsum, anhydrite, halite, apatite, and aragonite (Gross 1977; Milodowski et al. 2001; Elie et al. 2007).

Pure sulfate ettringite, calcium carbonates, and gypsum are rock-forming minerals in the lower part of the MZ sequence (Gross 1977; Clark et al. 1993; Milodowski et al. 2001). Unlike sulfate ettringite, its Cr-substituted analogs are rare in natural geological environment. As far as we know, the MZ is the only occurrence of these minerals. One is bentorite, a bright lilac Cr^{3+}-bearing ettringite, where Cr^{3+}substitutes for Al^{3+} in octahedra (Gross 1980), and the other is greenish-yellow, Cr-bearing ettringite (Figs. 2a and 2b). Gross (1977) was the first to attribute the color of Cr-bearing ettringite to the presence of Fe (up to 914 ppm) and Cr (up to 2080 ppm) impurities, but she did not discuss the Fe and Cr valence issues. As the yellow color produced by intense absorbance near 370 nm (Williams 1979) is a diagnostic feature of all chromates, we have inferred the presence of the CrO_4^{2-} chromophore oxyanion in the yellow Cr-bearing ettringites.

Calcite veins with abundant bentorite are known from the Hatrurim Basin, Maale Adummim, Hyrcania, and Nabi Musa complexes. Bentorite often occurs in association with truscottite, vaterite, jennite, tobermorites, afwillite, apatite, ettringite, and taumasite (Gross 1980). The fresh bentorite from Hatrurim that we studied is bright lilac and contains 1.919–1.985 apfu of Cr, i.e., it corresponds to pure Cr^{3+}-substituted ettringite (Table 2).

Abundant ettringite of various greenish-yellow shades is relatively widespread at two adjacent MZ localities of Maale Adummim and Nabi Musa. As seen in the field, the yellow color was the most intense in ettringite from the veins that cut CM rocks (Fig. 2a) that are rich in opaque minerals (brownmillerite, Fe-spinel, and Ca-ferrite) containing Cr^{3+} as an impurity (Figs. 3a and 3b). Perfect canary-yellow, prismatic crystals of ettringite (Figs. 3c and 3d; Table 2), together with afwillite, were restricted to the interior of monolith blocks of rock.

Hexavalent Cr-bearing ettringite and baryte-hashemite solid solutions occur also in the Maqarin Mottled Zone complex in

TABLE 2. Unit-cell parameters and crystal-chemical formulas of ettringite, Cr^{6+}-bearing ettringite, and bentorite based on calculation from EMPA data and quantification of EDX spectra

Locality (Sample)	Hatrurim Basin (Bent-1)			Maale Adummim (Ettr-1)			Maale Adummim (Ettr-5)			Nabi Musa (YV-2)			
Mineral	Bentorite			Ettringite			Cr^{6+}-bearing ettringite			Cr^{6+}-bearing ettringite			
Analysis	1	2	3	1	2	3	1	2	3	1	2	3	4
Si	0.024	0.039	0.039	0.001	0.000	0.003	0.657	0.644	0.568	0.013	0.012	0.042	0.008
Al	0.038	0.001	0.001	2.136	2.057	2.013	1.345	1.34	1.463	1.975	2.074	2.065	1.965
Fe	0.006	0.000	0.000	0.000	0.000	0.000	0.000	0.000	0.000	0.000	0.000	0.000	0.000
Cr^{3+}	1.919	1.985	1.979	0.003	0.020	0.014	0.000	0.000	0.000	0.000	0.000	0.000	0.000
Mg	0.007	0.009	0.009	0.008	0.005	0.003	0.005	0.001	0.006	0.009	0.010	0.010	0.010
Ca	5.865	5.908	5.892	5.763	5.737	5.833	5.987	6.017	5.987	6.073	5.730	5.880	5.820
Sr	0.002	0.000	0.000	0.021	0.021	0.023	0.001	0.000	0.001	0.031	0.020	0.020	0.020
Na	0.009	0.001	0.001	0.000	0.000	0.000	0.005	0.008	0.008	0.006	0.010	0.010	0.010
S	3.043	3.008	3.000	2.999	3.040	3.028	2.411	2.369	2.350	2.749	2.700	2.630	2.720
Cr^{6+}	0.000	0.000	0.000	0.000	0.000	0.000	0.315	0.352	0.351	0.215	0.290	0.300	0.310
$(SO_4)^{2-} + (CrO_4)^{2-}$	3.043	3.008	3.000	2.999	3.040	3.028	2.726	2.721	2.701	2.964	2.990	2.930	3.030
$Al + Cr^{3+} + Si$	1.981	2.025	2.019	2.140	2.077	2.030	2.002	1.984	2.031	1.988	2.086	2.107	1.973
Unit-cell parameters	$a = 22.455(1)$ $c = 21.489(4)$ Å $V = 9384.0(16)$ Å^3			$a = 11.2256(3)$ $c = 21.4367(14)$ Å $V = 2339.41(15)$ Å^3			$a = 11.2337(10)$ $c = 21.310(4)$ Å $V = 2329.0(4)$Å^3						

Notes: Formula based on 12 oxygen atoms, in apfu. K and Ti = 0.000 apfu.

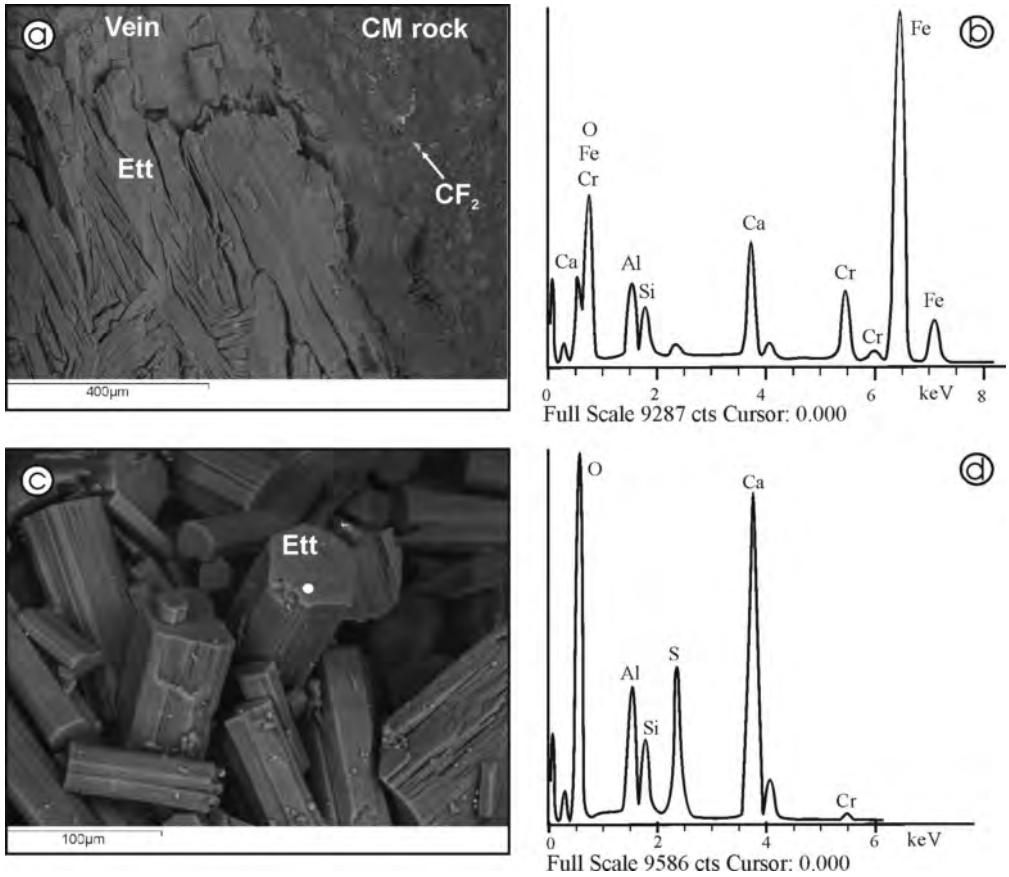

FIGURE 3. Backscattered electron images (BSE) of the minerals from the sample Ettr-5 (**a, c**) and characteristic EDX spectra of Cr^{3+}-rich calcium ferrite (**b**) and Cr^{6+}-bearing ettringite (**d**). (**a**) Contact of a Cr^{6+}-bearing ettringite and afwillite vein with a CM rock rich in opaque minerals. (**c**) Drusy aggregate of canary-yellow hexagonal prismatic crystals of Cr^{6+}-bearing ettringite filling the vein interior. Abbreviations: Ett = ettringite, CF_2 = calcium ferrite.

Jordan where Cr mineralization is associated with ongoing leakage of hyperalkaline solutions. Water sampled in the Maqarin area contains 0.5–5 mg/L of dissolved Cr^{6+}. Clark et al. (1993) believed that Cr^{6+} leached upon oxidation of the Cr^{3+}-bearing, opaque minerals in a hyperalkaline environment. The highest Cr content in the MZ rocks (from 780 to 9840 ppm) was measured in the leached Ca-rich CM rocks of Khyshaym Matruk, another Jordanian MZ complex (Elie et al. 2007). There, cryptocrystalline Cr_2O_3 is common at the base of the MZ strata, whereas the rocks altered by hyperalkaline waters contain Cr^{3+}, immobilized in volkonskoite, and Cr^{6+}, in baryte-hashemite solid solution (Fourcade et al. 2007).

Currently, chromatite has been found only as seasonal precipitates at the foot of Nabi Musa hill exposed in a road cut (Fig. 2c).

MATERIALS AND METHODS

Ten samples of the Nabi Musa rocks, including the CM rocks containing Cr-rich opaque minerals, low-grade Hatrurim rocks, different veins (Table 3), as well as two samples of chromatite precipitates (YV-1 and YV-2) and greenish-yellow ettringite from a 2 mm thick vein (sample YV-2) were collected for detailed analysis in 2007. Additionally, we selected samples of pure sulfate ettringite (Ettr-1) and canary-yellow Cr^{6+}-bearing ettringite (Ettr-5) from the Maale Adummim complex, and sampled bentorite from the Hatrurim Basin (Bent-1) (Table 4). The Maale Adummim and Hatrurim samples provide good reference for comparison as, unlike the Nabi Musa site, ettringite and its Cr^{3+}- and Cr^{6+}-substituted analogs exist at those localities as large segregations in veins (Figs. 2a and 2b).

We analyzed natural samples of chromatite, bentorite, and both sulfate and Cr^{6+}-bearing ettringite by optical microscopy, electron microprobe analysis (EMPA), scanning electron microscopy (SEM), energy-dispersive X-ray (EDX) spectroscopy, Fourier transform infrared (FTIR) spectroscopy, and X-ray powder diffraction (XRPD) methods [at the Sobolev Institute of Geology and Mineralogy (IGM) and Novosibirsk State University, Novosibirsk]. The instruments we used were a Thermo Scientific ARL X'TRA X-ray powder diffractometer, equipped with a Peltier cooled Si(Li) solid-state detector (Cu$K\alpha$ radiation), a LEO 420 and a JSM 6510LV SEM, and Camebax-Micro and JXA-8100 electron microprobes for EMPA procedures.

The EMPA measurements were conducted with an accelerating voltage of 20 kV, the peak count time was 10 s, the beam current was 20 nA, and the beam diameter was 2–3 μm for anhydrous minerals. Volatile-rich phases were analyzed at an accelerating voltage of 20 kV, a lower beam current (10 nA), a shorter peak count time (5 s), and a larger beam diameter (10 μm) to minimize beam damage to the minerals.

The X-ray powder diffraction analysis was performed using powdered silicon as the internal standard (a = 5.4309 Å). A step-scan mode data collection was employed using a step size of 0.02° and a 4 s count time per step. The 2θ range was 5–60°. The results were processed with WinXRD 2.0–6 (Thermo Scientific), and the unit-cell lattice parameters of ettringites were refined in GSAS (Larson and Von Dreele 2000).

The FTIR absorption spectra were recorded at room temperature on a Bruker VERTEX 70 FTIR spectrometer over the range 400–4000 cm^{-1}, with a resolution of 2 cm^{-1}. The pulverized samples, in 8 mg aliquots, were mixed uniformly with 800 mg KBr and pelletized.

Bulk major and trace element compositions were analyzed by inductively coupled plasma atomic emission spectroscopy (ICP-AES) and inductively coupled plasma mass spectrometry (ICP-MS) to an accuracy of 2–5% and 10%, respectively (Geological Survey of Israel, Jerusalem). Total element concentrations in solutions were determined by means of ICP-AES (IGM, Novosibirsk), to the same accuracy (Nikolaeva et al. 2008).

Spectrophotometric determination of CrO_4^{2-} oxyanion in aqueous solutions was performed following the procedure described by Jeffery (1970). A model Zeiss Specord M40 spectrophotometer was used for all spectra recording with matched 1 cm quartz cells. Absorbance was measured at 370 nm. All the measurements were made at 20°C in triplicate, and the results were expressed as the mean of the three measurements.

MODELING

Thermodynamic modeling at 25 °C and 1 bar total pressure was performed with the "HCh" code and the UNITHERM database using a free energy minimization algorithm (Shvarov 1999). We modeled the heterophase 15-component system H-O-C-Al-Cl-S-Na-K-Ca-Mg-Ba-Cr-Fe-Mn; the dissolved Cr^{6+}-species and its solid phases were incorporated into the model using data borrowed from the literature (Table 5).

Activity coefficients were calculated with the third approximation of the Debye-Hückel equation, which is valid for the ionic strength I < 0.5 mol/L. At a higher ionic strength of solution in equilibrium with NaCl and $CaCrO_{4(s)}$, the activity coefficients were calculated with the Helgeson equation (Helgeson et al. 1981):

$$\lg \gamma_i = -\frac{A \cdot z_i^2 \cdot \sqrt{I}}{1 + B \cdot \mathring{a}_i \sqrt{I}} - \lg(1 + 0.018 m^*) + [\omega_i b_{NaCl} + b_{Na^+Cl^-} - 0.19(|z_i| - 1)] \cdot I \quad (1)$$

TABLE 3. Major (wt%) and trace element (ppm) compositions of "low-grade Hatrurim" rocks, veins, paralava, and hydrothermally altered combustion metamorphic rocks from the Nabi Musa dome

Rock	"Low-grade Hatrurim" rocks			Veins			Altered CM rocks			Paralava
Sample	4	8ye	11	1wt	8wt	9gr	2	13	22	12D
SiO_2	6.90	39.30	5.60	1.70	34.90	1.50	25.20	24.60	8.10	36.00
TiO_2	0.10	<0.05	<0.05	<0.05	<0.05	<0.05	0.50	0.29	0.15	0.42
Al_2O_3	2.00	<0.10	0.90	0.70	0.10	0.70	9.80	10.10	4.40	6.00
Fe_2O_3*	1.00	0.20	0.60	0.10	0.20	0.40	4.50	4.00	2.40	2.80
MgO	1.00	0.20	0.50	0.30	0.20	52.20	14.90	0.60	0.50	1.00
CaO	46.70	42.90	49.00	52.90	43.60	9.80	17.00	45.80	47.20	48.10
Na_2O	0.50	0.80	1.20	0.30	0.40	0.50	1.60	0.30	0.50	0.40
K_2O	<0.10	0.30	0.30	<0.10	<0.10	<0.10	0.20	0.20	<0.10	0.20
P_2O_5	2.50	0.10	2.80	0.20	<0.10	0.50	3.90	2.90	1.90	1.10
SO_3	10.00	<0.20	5.00	3.40	<0.20	0.30	2.80	1.30	1.20	0.20
CO_2	24.61	5.87	31.66	37.26	18.83	11.23	6.84	3.13	n.a.	1.51
Cl	0.34	0.51	0.39	0.26	0.56	1.14	n.a.	<0.015	0.11	0.06
H_2O^+	3.85	10.22	2.55	2.58	1.41	21.0	12.63	6.45	n.a.	1.43
LOI	28.80	16.60	34.60	40.10	20.80	33.60	19.50	9.60	33.10	3.00
Total	99.67	100.40	100.80	99.70	100.60	99.50†	99.90	99.69	99.45	99.23
B	97	79	9.4	8	n.a.	207	n.a.	n.a.	17	81
Se	26	4	3	3	<2	15	4	10	24	<2
Sr	500	1500	680	140	400	140	1000	1100	1200	1500
Ba	490	120	40	22	90	<5	90	340	407	610
Cr	400	420	25	34	315	1200	135	565	265	250
Ni	190	13	95	46	16	30	250	365	175	165
Mn	<100	<100	<100	<100	<100	<100	<100	<100	<100	100
V	115	2	36	10	3	52	225	180	70	105
Zn	175	33	45	17	17	100	425	1025	15	1050
Mo	20	1	10	2	3	800	14	19	14	5.6
U	29.0	0.6	9.0	1.2	0.9	4.6	78.0	7.0	30.0	50.0
Th	1.2	<0.1	0.4	0.2	<0.1	0.4	2.6	3.3	1.2	1.3

Note: n.a. = not analyzed.
* All iron analyzed as Fe_2O_3.
† Total includes F – 0.23 wt%.

TABLE 4. Main characteristics of the studied samples

MZ area	Rock type	Sample	Mineral assemblage	
			Main phases	Minor phases
Nabi Musa	Paralava	12D	Rnk, Mll	Pwo, Wo, Lrn, Csp, Nag, Ap-(CaF), Ti-rich andradite, Hem, Ett, Cat
	Altered CM rocks	2	Arg, Spu, Ell-(F)	Cat, Gp, PBss, Fe-spl
		13	Mll, Lrn, Cat, Tob	Ti-rich andradite, Prv, CF2, Csp, Ap-(CaF)
		22	Cat, Brmt	Tob
	"Low-grade Hatrurim rocks"	4	Cat, Gp	Qz
		8ye	Cat, Vtr, Tob	–
		11	Cat, Gp	–
	"Low-grade Hatrurim rocks" with chromatite precipitates	YV-1	Cat, Arg, Gp, Chr	Hl, Qz
		YV-2	Cat, Arg, Gp, Chr	Cr^{6+}-bearing Ett, Hl, Brt-Hsh ss, Qz, Ell-(OH)
	Veins	1wt	Cat, Gp	–
		8wt	Cat, Tob, Vtr	Arg
		9gr	Brc, Cat	Hl, Cr^{6+}-bearing Ett
Maale Adummim	Veins	Ettr-1	Ett	–
		Ettr-5	Cr^{6+}-bearing Ett	Afw
Hatrurim Basin	Vein	Bent-1	Bent	Prt, Jen, Cat

Note: Arg = aragonite, Afw = afwillite, Ap-(CaF) = apatite, Brc = brucite, Brmt = brownmillerite, Brt-Hsh ss = baryte-hashemite solid solutions, Cat = calcite, CF_2 = calcium ferrite, Chr = chromatite, Cr^{6+}-bearing Ett = Cr^{6+}-bearing ettringite, Csp = cuspidine, Ett = ettringite, Ell-(F) = ellestadite-(F), Ell-(OH) = ellestadite-(OH), Fe-spl = Fe-spinel, Gp = gypsum, Hem = hematite, Hl = halite, Jen = jennite, Lrn = larnite, Mll = melilite, Nag = nagelschmidtite, PBss = perovskite–brownmillerite solid solution, Prt = portlandite, Prv = perovskite, Pwo = pseudowollastonite, Qz = quartz, Rnk = rankinite, Spu = spurrite, Tob = tobermorite, Vtr = vaterite, Wo = wollastonite.

TABLE 5. Solid phases and chromium species potentially present in Nabi Musa rock complex and their Gibbs free energy of formation

Species and Minerals	$\Delta_f G^0_{298}$, kcal/mol	Reference
$CaCrO_4^0$	–309.838	Perkins and Palmer (2000)
Brownmillerite	–1260.62	Geelhoed et al. (2002)
Cr-brownmillerite	–1260.62	Geelhoed et al. (2002)
Chromatite	–310.564	Wang and Li (2004)
Cr-spinel	–398.919	Robie et al. (1978)
CSH, CaH_2SiO_4	–424.752	Geelhoed et al. (2002)
Hydrocalumite	–2256.89	Damidot and Glasser (1993)
Cr^{6+}-hydrocalumite	–2367.35	Perkins and Palmer (2001)
Cr^{6+}-ettringite	–3616.40	Perkins and Palmer (2000)
Ettringite	–3635.52	Perkins and Palmer (1999)
Hashemite	–321.31	Rai et al. (1988)
Hydrogarnet	–1199.15	Wazne et al. (2008)
Tobermorite	–2361.451	Kulik and Kersten (2001)

where γ_i is the molal activity coefficient, m^* is the summation of molal concentrations Σm_i, ω_i is the absolute Born parameter, and b_{NaCl} is the solvation parameter. The first term of Equation 1 includes the Debye-Hückel parameters A, B, $å$, the charge of a species z, and the ionic strength I.

CHROMIUM IN NABI MUSA ROCKS AND MINERALS

Chromium in rocks

The diverse brecciated rocks that form the Nabi Musa melange show quite a wide range of Cr contents (Table 3). Chromium contents range from 135 to 565 ppm in Ca-rich CM rocks, where the highest Cr content is in the rock varieties rich in opaque minerals (samples 13 and 22). In the low-grade Hatrurim rocks, Cr contents range between 25 and 420 ppm. The pieces with the highest Cr concentrations are easily spotted as they have a yellow-greenish color (sample 8ye). Veins show the broadest range of Cr concentrations: the lowest concentration of 34 ppm (sample 1wt) is found in carbonate veins, which may be of calcite, aragonite, or vaterite; CSH (tobermorite) veins may contain up to 315 ppm (sample 8wt); and in bright green or yellow-green brucite veins that bear minor amounts of calcite, halite, and fine ettringite impregnation (sample 9gr) Cr concentrations are as high as 1200 ppm.

Cr^{6+}-bearing minerals

Chromatite. We failed to see traces of chromatite during our first trip to the Nabi Musa outcrop in March 2007. It was the last rainy month in the Judean Desert, with a mean air temperature about 20 °C. Two months later, however, in May 2007, we did find lemon-yellow, powder-like and canary-yellow, fine-grained precipitates encrusted on cracks and on rock debris surfaces at the foot of the hill (Fig. 2c). During this hot season, the daytime air temperature rises to 40–45 °C and the soil temperature runs up to 60 °C (Goldreich 2003).

The XRPD patterns of the powder-like precipitates are identical to that of the PDF card ICDD 8-458 ($CaCrO_4$, $I4_1/amd$). The a (7.25 Å) and b (6.30 Å) values determined for the Nabi Musa chromatite approach those of synthetic compounds (ICDD 8-458) and Zabierzów chromatite (Bajda 2005). Chromatite is lemon-yellow and has a vitreous luster. Cleavage is obscure. In thin sections, the mineral is yellow, non-pleochroic, with strong dispersion. It is easily soluble in water yielding a yellow solution. The canary-yellow, fine-grained aggregates consist of rare U- and V-bearing minerals, namely tyuyamunite and strelkinite.

The precipitates of calcium chromate (2–20 μm grain size) in the Nabi Musa outcrop are of three morphological types: (1) flattened "flake-like" forms with uneven margins (Fig. 4a); (2) delicate overgrowths that coat corroded grains of calcite and/or gypsum (Figs. 4b and 4c); or (3) numerous imperfect chromatite crystals that encrust the corroded surfaces of gypsum and calcite. Crystals of the last type are usually aggregated and serve as seeds for chromatite of later generations. Chromatite forms shortened prismatic grains and tetragonal bipyramids (Figs. 4d and 4e). The Nabi Musa chromatite crystals are generally rather similar to those reported from Zabierzów, Poland, found in soils polluted with electroplating effluents (Bajda 2005). On the other hand, they differ markedly from the perfectly faceted chromatite crystals (up to 100 μm in size) of the adjacent Maale Adummim locality (Gross 1977).

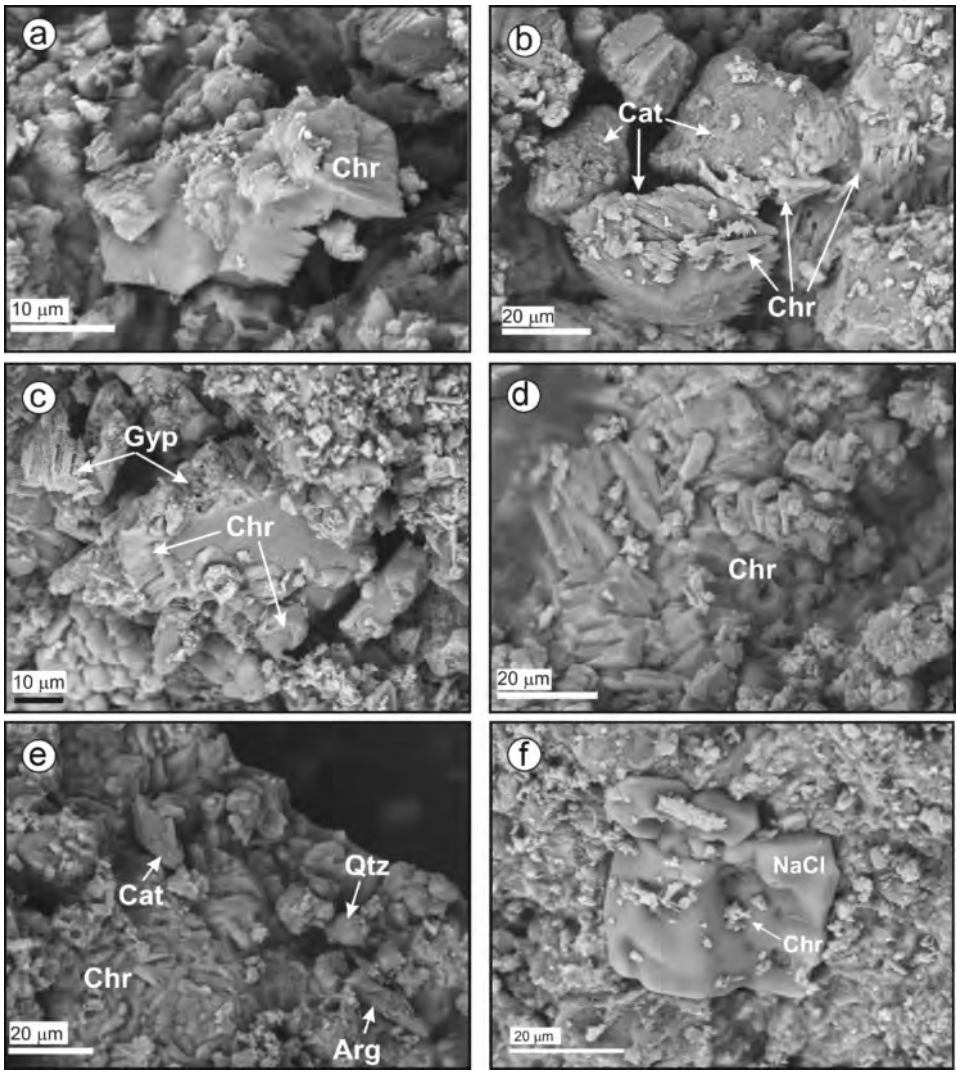

Figure 4. SEM images that illustrate the morphological diversity of calcium chromate precipitates and associated minerals. Sample YV-1. (**a**) $CaCrO_4 \cdot 2H_2O$ "flakes" with uneven margins (type 1). (**b, c**) Chromatite crystals coating corroded grains of calcite and/or gypsum (type 2). (**d**) Tabular habit of chromatite crystals faceted by short tetragonal bipyramids and prisms (type 3). (**e**) Chromatite accompanied by scalenohedral calcite crystals and pseudo-hexagonal prismatic aragonite twins from encrustations on crack walls; quartz grain coated with calcium chromate film. (**f**) Halite individual encrusted by fine-grained precipitates of chromatite. Abbreviations: Arg = aragonite, Cat = calcite, Cht = chromatite, Gp = gypsum, Qtz = quartz, Hl = halite.

The calcium chromate precipitates were investigated by SEM/EXD quantitative chemical analysis and showed different ratios of peak intensities of Ca, Cr, and O in the EDX spectra, which correspond to different element ratios, in the "flakes" and in crystals of chromatite. The crystals were identical in composition to anhydrous $CaCrO_4$ (Fig. 5a), whereas the ratios between Ca, Cr, and O in the flakes were close to those in calcium chromate dihydrate ($CaCrO_4 \cdot 2H_2O$) (Table 6). Both phases contained a sulfur impurity.

The chromatite precipitates that encrust loose surficial rock debris, including fragments of the MZ melange, are associated mainly with calcite and gypsum. Occasionally, quartz and plagioclase grains are coated with calcium chromate films (Fig. 4e). Crystals of other minerals are commonly co-precipitated with chromatite in cracks. Aragonite is a major phase of these assemblages; it exists as flattened prismatic or rod-like crystals, and is typically twinned (Fig. 4e). Late calcite occurs as scalenohedral crystals (Fig. 4e). Rounded halite grains coat the surfaces of microfractures and may act as seeds for chromatite precipitation (Fig. 4f). Ellestadite-(OH) (Fig. 5b), existing as prismatic, hopper-like crystals, is rare in this assemblage. Hashemite and baryte-hashemite solid solution (Fig. 5c) were found as several microcrystals. A single grain of Cl-enriched hydrogarnet was determined from an EDX spectrum (Fig. 5d).

Ettringite. Most ettringite inside the Nabi Musa edifice is colorless or white, existing in thin continuous veins that are hosted by the low-grade Hatrurim rocks. It forms columnar, fibrous, or prismatic aggregates that grow perpendicular to vein walls, usually straddling the vein from one wall to the other. It corresponds in composition to pure sulfate ettringite and is free of Cr (Figs. 6a

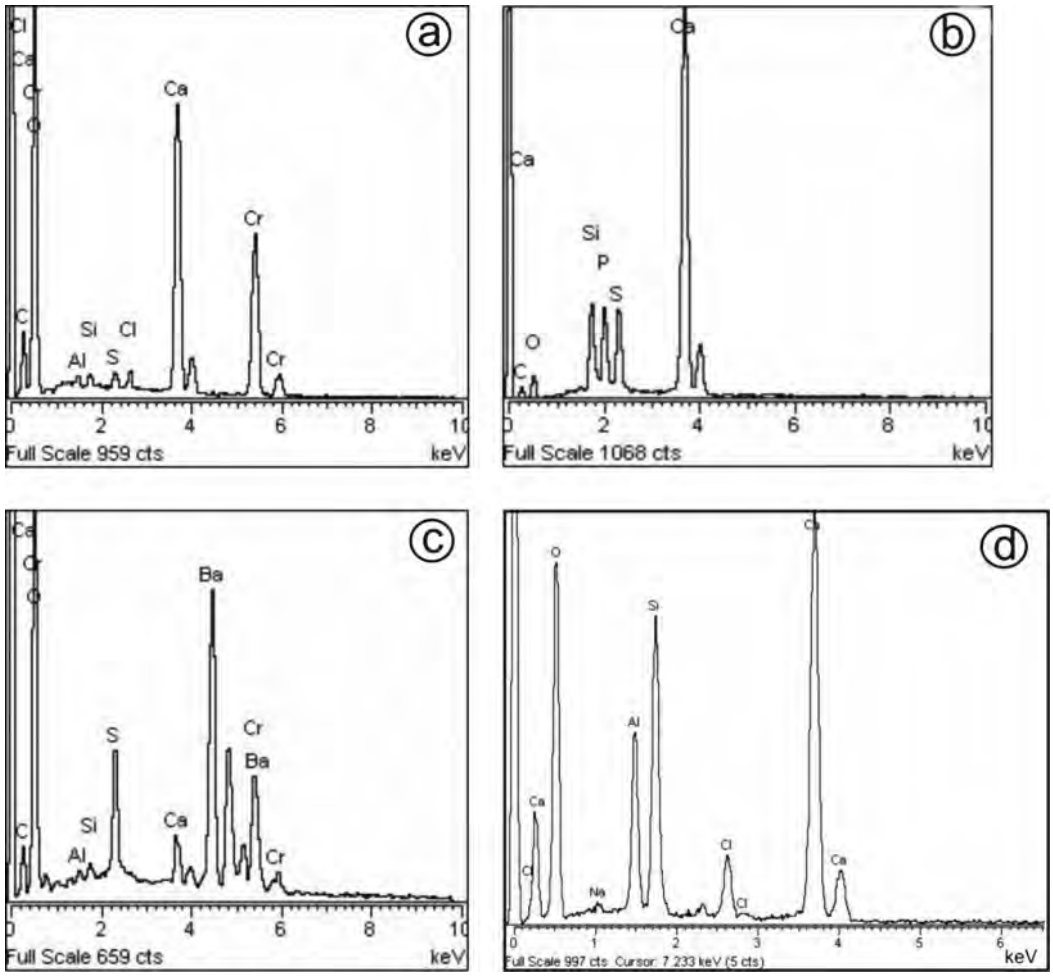

FIGURE 5. Characteristic EDX spectrum of chromatite (**a**) and associated minerals: ellestadite-(OH) (**b**), barite-hashemite solid solution (**c**), and Cl-bearing hydrogarnet (**d**).

TABLE 6. Chromatite and calcium chromate dihydrate compositions

Sample:	$CaCrO_4$		$CaCrO_4 \cdot 2H_2O$	
	1	2	1	3
Measured element concentrations				
Ca	25.64	24.63	20.83	20.94
Cr	33.33	31.53	27.08	25.05
O	41.03	41.20	50.00	51.33
S	–	1.24	–	0.74
H	–	n.a.	2.08	n.a.
Total	100.00	98.60	99.99	98.06
Calculated compositions				
CaO	35.90	34.47	29.14	29.30
CrO_3	64.10	60.64	52.08	48.17
SO_3	–	3.09	–	1.85
H_2O	–	–	18.56	21.08
Total	100.00	98.20	99.78	100.40

Notes: 1 = Theoretical composition, 2 = crystal, 3 = flake-like individual.
n.a. = not analyzed.

and 6b). The greenish-yellow ettringite is rare and exists either as impregnations (sample 9gr) or as small veins, 0.5–2 mm thick (sample YV-2). It occurs in thin, zoned veins with small (up to 0.5–1 mm) vugs that enclose long, hexagonal prisms $\{10\bar{1}0\}$ of greenish-yellow ettringite, terminated by pinacoid {0001} or rarely by low pyramids (Fig. 6c); fresh crystals have perfect cleavage parallel to the long hexagonal prisms $\{10\bar{1}0\}$, which is often displayed as a corresponding striation of prismatic crystals along the *c* axis. The zoned veins have afwillite (lath-like crystals or herringbone aggregates) and sulfate ettringite (Fig. 6a) on their periphery; calcite crystals lie along the boundary between these veins and the low-grade Hatrurim host rocks. The matrix of the host rocks near the veins may bear CSHs, Cl-bearing ellestadite-(OH), and a fine impregnation of sulfate ettringite, in addition to the predominant calcium carbonates and gypsum.

The EDX spectra and electron microprobe analyses of the greenish-yellow ettringite crystals from Nabi Musa show limited Cr (0.215–0.310 apfu) and Si (0.008–0.042 apfu) substitutions (Table 2; Fig. 6d). According to our crystal-chemical calculations, Cr in the analyzed ettringites is mostly hexavalent chromium. The presence of Si in the ettringite is most probably because of limited ettringite-thaumasite solid solution that is similar to that seen in synthetic compounds, as reported by Macphee and Barnett (2004).

The green-yellowish ettringite from lenses and knots in the Nabi Musa brucite veins (sample 9gr) has a different composition and habit. Its BSE image illustrates numerous shrinkage cracks due to drying (Fig. 7) and its EMPA analyses showed the range of Cr_2O_3 contents from 0.3 to 2.7 wt%.

EDX and EMPA are not able to determine the Cr valence, so we applied XRPD and FTIR spectroscopy to investigate whether

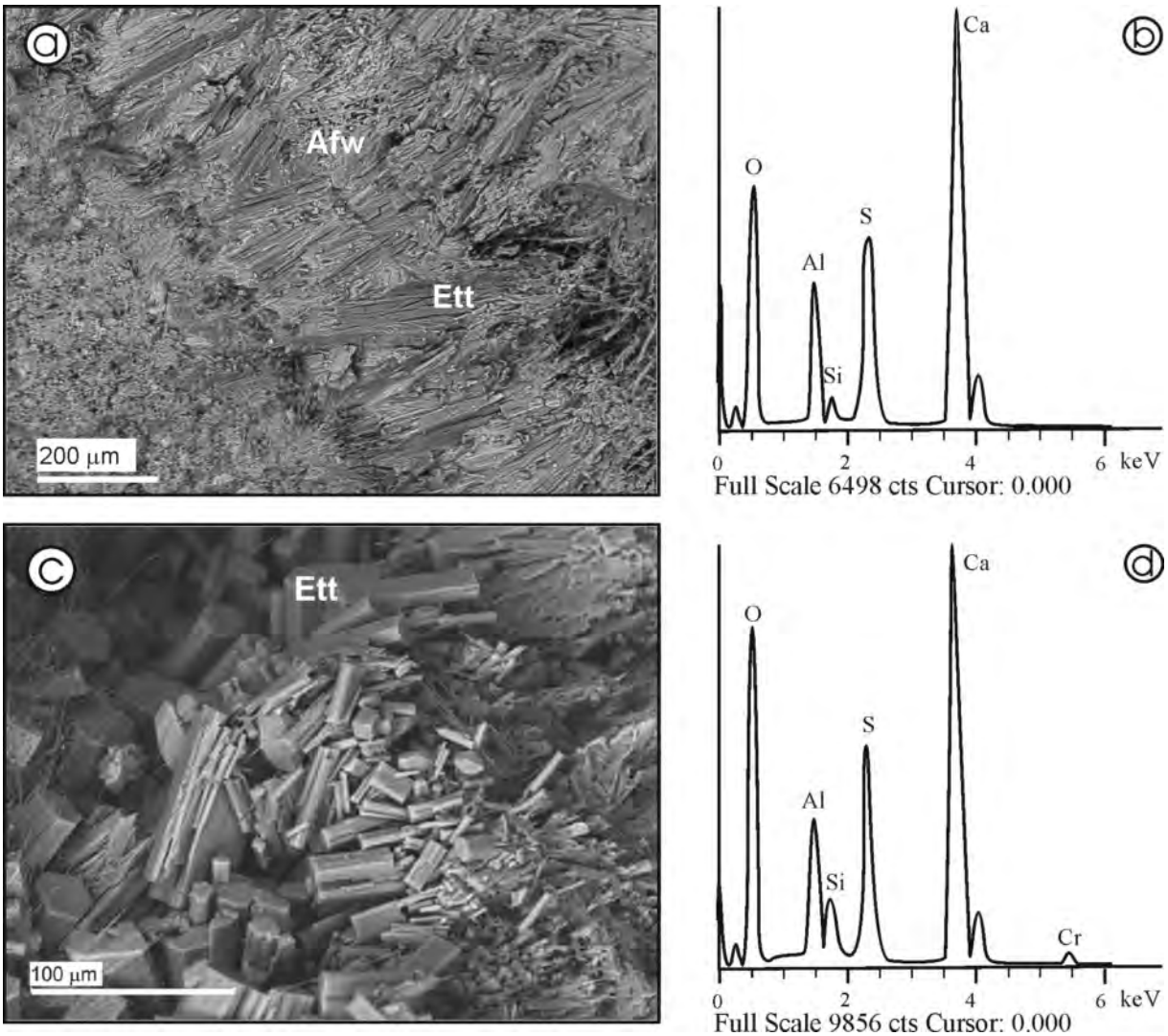

Figure 6. Backscattered SEM images and respective characteristic EDX spectra of sulfate ettringite (**a, b**) and Cr^{6+}-bearing ettringite (**c, d**) from Nabi Musa. (**a**) Typical herringbone structure composed of afwillite and sulfate ettringite lining the vein wall in low-grade Hatrurim rock. (**b**) Characteristic EDX spectrum of pure sulfate ettringite. (**c**) Fine-grained prisms of fresh Cr^{6+}-bearing ettringite from the vein interior. (**d**) Characteristic EDX spectrum of Cr^{6+}-bearing ettringite. Abbreviations: Afw = afwillite, Ett = ettringite.

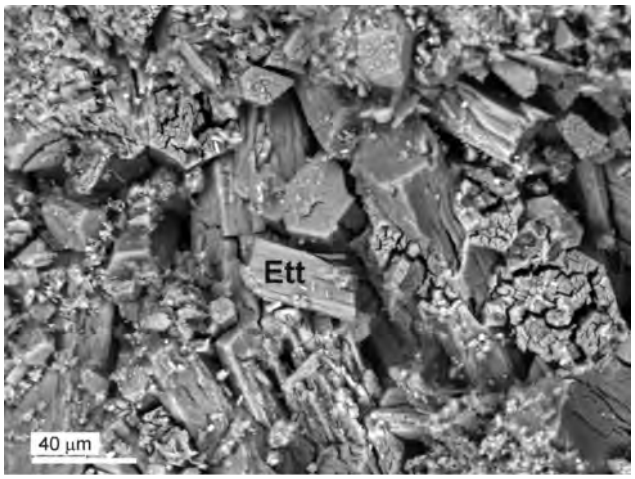

Figure 7. Backscattered SEM image of cracked and dehydrated Cr^{6+}-bearing ettringites from Nabi Musa MZ complex.

it is the cations (Cr^{3+}) or the anions CrO_4^{2-} that incorporate in the ettringite-type phases from the MZ complexes.

XRPD data. The unit-cell parameters of the measured samples Ettr-1, Ettr-5, and Bent-1 are given in Table 2. The unit-cell parameters of bentorite (Bent-1) were slightly larger than those in the literature (Gross 1980), which may be a consequence of environmental effects, especially moisture. The unit-cell parameters of natural sulfate ettringite (Ettr-1) were similar to those of its synthetic analog (Poellmann et al. 1993). A slightly smaller value *c* in the sample of Ettr-1 may be due to its lower H_2O content. Sample Ettr-5, with the highest Cr^{6+} concentrations of all the ettringites that we have studied (up to 0.352 apfu Cr) had a notably smaller unit-cell volume than that of its synthetic analog (Poellmann et al. 1993), possibly because of a significant amount of Si (up to 0.657 apfu) in the mineral. It was impossible to infer the structural position of Cr in these ettringites by means of XRPD because of minor substitution of CrO_4^{2-} for SO_4^{2-} and multi-component solid solutions. XRPD

is more informative for comparing synthetic phases that grow under controlled experimental conditions and that are solid solutions between the sulfate ettringite and chromate ettringite end members (Terai et al. 2006; Poellmann et al. 1993).

FTIR data. CrO_4^{2-} anions in all chromate-bearing solid species can be recognized by infrared spectroscopy. $CaCrO_4$, which is isostructural with $ZrSiO_4$, has the space group $I4_1/amd - D_{4h}^{19}$, with Z = 4. The site symmetry of Cr that is in tetrahedral coordination with oxygen is D_{2d} (Doyle and Eddy 1967). The FTIR spectrum of natural chromatite (Fig. 8) is consistent with the D_{2d} site symmetry. No band is observed corresponding to ν_1. The strong, sharp band at 877 cm^{-1} is assigned to the ν_3 CrO_4 vibration. Minor additional bands observed at 669, 713, and 856 cm^{-1} are probably due to CO_3^{2-} vibrational modes of aragonite (Nakamoto 1997), which is present as an impurity in chromatite powder precipitates.

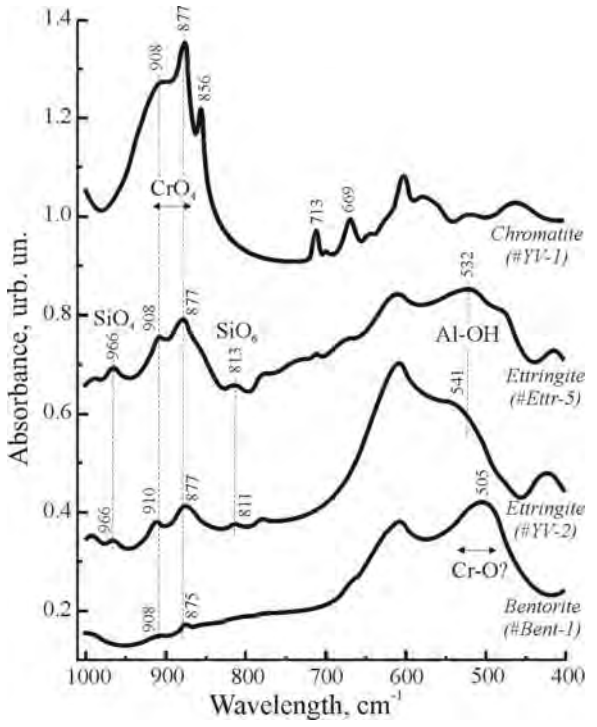

FIGURE 8. FTIR spectra of chromatite, bentorite, and Cr^{6+}-bearing ettringites in KBr pellets (interpretation based on Doyle and Eddy 1967; Perkins and Palmer 2000; Gastaldi et al. 2009).

The FTIR spectra of these natural CrO_4^{2-}-bearing ettringites agree well with those in earlier studies of the synthetic chromate analog of ettringite (Perkins and Palmer 2000) and pure sulfate ettringite (Gastaldi et al. 2009). The wide band ranging from 860 to 910 cm^{-1} (Fig. 8) in the spectra of the canary-yellow ettringite from Maale Adummim (Ettr-5) and the green-yellowish ettringite from Nabi Musa (YV-2) is typical of the SO_4–CrO_4 intermediate phase (Perkins and Palmer 2000). The spectrum of Ettr-5 with ~0.35 apfu Cr^{6+} bears a distinct individual absorbance band centered at 877 cm^{-1} attributable to the CrO_4 ν_3 vibration. This band is more diffuse in YV-2, which has a lower Cr^{6+} concentration of ~0.2–0.3 apfu, and is absent from the spectrum of Cr^{3+}-substituted ettringite–bentorite (Bent-1). One of the strongest complex vibrational bands ranges from 523 to 620 cm^{-1} appears in the spectra of both Cr^{6+}-bearing ettringites. We attribute this band to an Al-OH bending vibration, following the previous assignment of Perkins and Palmer (2000).

Minor bands at 811–813 cm^{-1} and 966 cm^{-1} are observed uniquely in the spectra of CrO_4^{2-}-bearing ettringite. Both bands are produced by silicon in the ettringite structure (Table 2). Macphee and Barnett (2004) interpreted that the bands near 820 and 966 cm^{-1} are due to octahedrally coordinated Si and the SiO_4-group in ettringite-thaumasite solid solution, respectively.

Cr^{3+}-bearing opaque minerals from CM rocks

Three typical CM rocks that differ by their mineral and chemical composition were selected for a detailed study (Table 7), namely brownmillerite marble (sample 22), gehlenite-larnite hornfels (sample 13), and spurrite marble (sample 2).

Brownmillerite is the only opaque mineral that occurs in marble (sample 22). Its major components are Fe_2O_3, CaO, and Al_2O_3, with other oxides existing as impurities (in wt%): these are MgO (1.19–1.47), TiO_2 (1.09–1.89), SiO_2 (0.34–0.37), MnO (to 0.19), and NiO (to 0.08) (Table 7). The concentration of Cr_2O_3 in brownmillerite varies from 0.04 to 2.55 wt%. Zinc is below its detection limit (<0.03 wt% ZnO).

Fe-spinel is a main opaque phase in spurrite marble (sample 2). Grains ranging in size from 50 to 200 μm are enriched in

TABLE 7. Representative analyses of opaque minerals from Nabi Musa CM rocks

Sample	22		13						2					
Mineral	Brmt	Brmt	Prv	Prv	CF_2	CF_2	Fe-spl (c)	Fe-spl (r)	Fe-spl†	Fe-spl†	Fe-spl‡	Fe-spl‡	PBss	PBss
SiO_2	0.34	0.37	2.32	2.92	7.79	7.98	0.00	0.00	0.00	0.00	0.13	0.00	4.70	5.04
TiO_2	1.89	1.09	41.60	40.90	0.99	0.79	0.00	0.00	0.33	0.28	0.35	0.12	12.90	12.92
Cr_2O_3	2.55	0.04	1.21	1.10	0.21	0.47	5.46	3.76	2.98	6.42	0.27	0.29	0.08	0.18
Al_2O_3	21.63	23.15	0.55	0.63	6.06	4.84	2.88	2.87	12.18	12.78	11.99	10.41	3.26	3.33
FeO	–	–	–	–	–	–	10.32	9.92	3.50	2.89	2.13	1.74	–	–
Fe_2O_3*	23.08	25.65	11.30	10.84	66.30	67.38	69.42	71.23	65.22	61.40	68.01	71.79	30.86	29.59
MnO	0.05	0.19	b.d.	b.d.	0.03	0.00	0.15	0.17	b.d.	b.d.	0.00	0.00	n.a.	n.a.
MgO	1.47	1.19	0.04	0.07	3.24	2.79	10.09	10.45	19.26	19.76	17.58	20.11	0.30	0.41
CaO	47.66	48.38	41.78	41.81	13.46	13.60	0.24	0.60	0.82	0.80	4.54	1.05	42.48	43.50
CuO	n.a	n.a.	n.a	n.a.	n.a	n.a.	1.08	1.08	0.05	0.11	0.07	0.15	n.a	n.a.
NiO	0.08	0.04	0.02	0.04	0.14	0.14	3.12	2.91	0.90	0.90	0.74	0.93	n.a	n.a.
ZnO	b.d.	b.d.	b.d.	b.d.	0.30	0.30	4.62	4.06	0.20	0.20	0.15	0.18	n.a.	n.a.
Total	98.61	100.10	98.81	98.27	98.52	98.28	100.16	99.71	99.28	99.77	99.68	100.20	94.58	94.97

Notes: b.d. = below detection, n.a. = not analyzed, (c) = core, (r) = rim.
Brmt = brownmillerite, CF_2 = calcium ferrite, Fe-spl = Fe-splinel, PBss = perovskite-brownmillerite solid solution, Prv = perovskite.
* All iron analyzed as Fe_2O_3, FeO, and Fe_2O_3 calculated from mineral stoichiometry.
† Grains form 50 up to 200 μm in size.
‡ Grains from 5 up to 10 μm in size.

Cr (2.98–6.42 wt% Cr_2O_3), whereas very small grains (5–10 μm in size) have Cr_2O_3 concentrations below 0.29 wt% (Table 7). Fe-spinel also concentrates Ni (0.74–0.93 wt% NiO), Zn (0.15–0.20 wt% ZnO), and Cu (0.05–0.11 wt% CuO), but lacks manganese. The same sample comprises several grains of perovskite-brownmillerite solid solution with 0.08–0.18 wt% Cr_2O_3 (Table 7).

The hornfels sample 13 contains a diverse assemblage of opaque minerals. Perovskite and Fe-spinel are present in a similar quantity (about 5 vol%), but calcium ferrite is restricted to few grains. Fe-spinel shows the highest content of Fe_2O_3 (69.42–71.23 wt%) and MgO (10.09–10.45 wt%). The other components include 3.76–5.46 wt% Cr_2O_3, 2.91–3.12 wt% NiO, and 4.06–4.62 wt% ZnO; Al_2O_3 is below 2.88 wt%, MnO is between 0.15 and 0.17 wt%, and TiO_2 is below the detection limit (<0.01 wt%). Thus, Fe-spinel is represented by the multi-component solid solution $FeFe_2O_4$–$(Mg,Zn,Ni)(Cr,Al)_2O_4$. Perovskite commonly contains impurities of Cr_2O_3 (1.10–1.21 wt%), SiO_2 (2.32–2.92 wt%), and Al_2O_3 (0.55–0.63 wt%) (Table 7). Calcium ferrite shows a rather regular composition (in wt%): Fe_2O_3 (66.30–67.38), CaO (13.46–13.60), SiO_2 (7.79–7.98), Al_2O_3 (4.84–6.06), TiO_2 (0.79–0.99) and contains Cr, Ni, and Zn as impurities (in wt%): Cr_2O_3 (0.21–0.47), NiO (0.14), ZnO (0.30) (Table 7).

Batch experiments

We performed batch tests on Cr leaching from rock (sample 9gr, the sample with the highest total Cr content) to determine the valence and the concentrations of Cr that dissolve as the Nabi Musa rocks interact with rain water. For the experiments, 2 and 5 g aliquots of pulverized rock were suspended in a total volume of 10 mL distilled deionized water (pH = 7) yielding the liquid/solid ratio (LS) of 5 and 2, respectively, to simulate the conditions of Cr leaching under the atmospheric conditions. Table 8 shows the aqueous concentrations after leaching for 7 days. The pH values were about 9.5, and we measured both Cr^{3+} and Cr^{6+} in the solutions. The aqueous Cr concentrations varied with LS (ppm) from 1.53 (at LS = 5) up to 3.69 (at LS = 2), which is an indication of no mineral solubility control. The data presented in Table 8 show that all Cr in the solutions at pH = 9.5 exists as hexavalent chromium.

Figure 9 shows the absorption spectra of the solutions after the batch experiments. The spectra were recorded from 4000 to 1200 cm^{-1}. The spectrum of a standard solution containing 1.7 mg/L of Cr^{6+} at pH = 9.5 was also recorded. No species of Cr other than CrO_4^{2-}, which has maximum absorptions at 275 and 370 nm, is required to explain the spectra of the leach solutions.

TABLE 8. Results of batch experiments

Elements	Concentration in solution, ppm	
Mg	510	1090
Na	542	1400
Ca	7.9	10.3
Al	0.09	0.19
Fe	0.10	0.14
Cr_{total}	1.53	3.69
Cr^{6+}	1.48	3.80
Mo	1.33	2.92
B	15.2	24.5
S	29.1	75.9
Se	1.15	2.47
Si	0.21	0.35
pH	9.4	9.5
LS	5	2

Note: LS – liquid/solid ratio.

DISCUSSION

The MZ complexes are exceptional geological objects in which Cr mineralization is genetically related to diagenesis of metal-rich, marine sediments: Late Cretaceous organic-rich, sedimentary rocks have been the principal Cr source (Gross 1977; Gilat 1994, 1998; Bogoch et al. 1999). Chromium mobilization from the sediments and the formation of Cr^{3+}- and Cr^{6+}-bearing minerals were governed by diagenesis, combustion metamorphism, and later hydrothermal alteration of the MZ strata.

Maturation of organic-rich, marine sediments in the Cenozoic pull-apart basin of the Dead Sea produced limited amounts of oil and gas, whereas sediment compaction caused expulsion of abundant mineralized fluids (Gardosh et al. 1996; Gvirtzman and Stanislavsky 2000). In the Late Cenozoic, the latter process was accompanied by mud volcanism connected with over-pressured sedimentary strata on the periphery of the Dead Sea, and by repeated expulsions of compact hydrocarbon gas (mainly methane) and brines (Gilat 1998; Vapnik et al. 2007; Sokol et al. 2010). The expelled hydrocarbon gases are known to spontaneously ignite and burn for a long period, thus inducing combustion metamorphism of calcareous, or rarely marly, sedimentary rocks, which led to Cr^{3+} immobilization in Fe-spinel, brownmillerite, Ca ferrites, and perovskite (for details see Sharygin et al. 2008).

The setting changed dramatically when the activity of mud volcanoes decayed, and the expulsions of gas gave way to those of brines. CM rocks in the MZ complexes north of the Dead Sea basin were almost fully eliminated during later hydration and carbonation and were eventually converted into the so-called low-grade Hatrurim rocks. Modeling infers the equilibrium

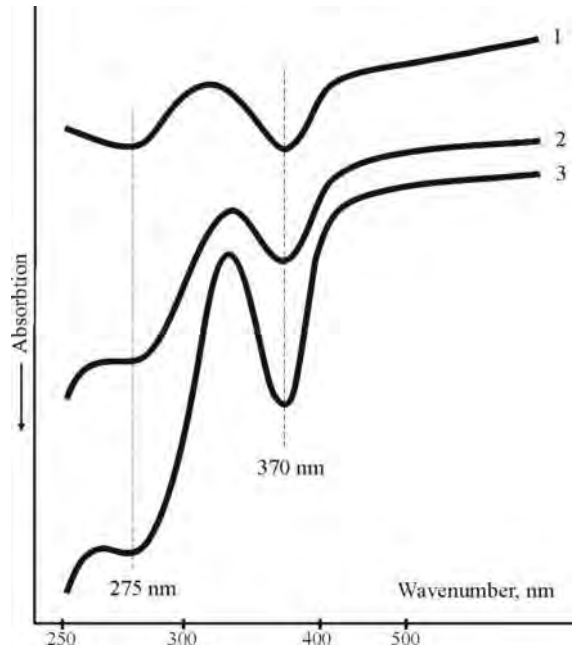

FIGURE 9. The UV-VIS absorption spectra of solutions. 1 = standard solution of Na_2CrO_4 with 1.7 mg/L Cr^{6+} under pH = 9.5; 2, 3 = solutions after batch experiments at LS ratios 5 and 2, respectively.

TABLE 9. Model scheme of the transformation of mineral paragenesis with equilibrium pH and element concentrations (mol/kg H_2O) under a set of supergene processes

Rock (sample)	Real assemblage	Modeling assemblage	pH	Aqueous concentration
"Low-grade Hatrurim" rock (8wt)	**Calcite**	**Calcite**	12.31	Ca = 7.3e-03
	Tobermorite	**Tobermorite**		Cr = 8.08e-04
	Vaterite	*Brucite*		Si = 1.25e-04
	Aragonite	*Hematite*		Mg = 4.31e-08
Vein (9gr)	**Brusite**	**Brusite**	12.09	Ca = 5.47e-02
	Calcite	**Calcite**		Cr = 2.73e-02
	Halite	**Halite**		Mg = 3.64e-07
	Cr^{6+}-ettringite	*Cr^{6+}-ettringite*		
		Gibbsite		
Precipitates (YV-1)	**Calcite**	**Calcite**	10.44	Ca = 6.28e-01
	Gypsum	**Gypsum**		Cr_{total} = 5.37e-01
	Chromatite	**Chromatite**		(CrO_4^{2-} = 1.58e-01;
	Hashemite	*Brusite*		$CaCrO_4^0$ = 3.6e-01)
	Halite	*Hashemite*		Mg = 6.53e-04
		Halite		Ba = 9.75e-08
				Na = 6.19e+00
				S_{total} = 9.09e-02
				(SO_4^{2-} = 1.69e-02)

Note: Bold and italic are major and minor phases, respectively.

brines reached pH as high as 12.31 (Table 9).

The portlandite-buffered composition of aqueous solutions is uncommon for source layers and reservoirs of mud volcanoes (Kopf 2002). Normally, diagenesis of clay-rich sediment in high-pressure zones causes decomposition of carbonates, whereby Ca^{2+} and HCO_3^- dissolve into pore waters that also contain K^+ and Na^+ as principal cations. The rare group of natural, lime-saturated pore waters appears in a particular setting, namely, during diagenetic alteration of mainly calcareous deposits at shallow depths, in places where the sediments are drained through dense faults that strongly decrease pressure in the source layers (Kholodov 1993). As calcium carbonates decompose in this setting, gaseous CO_2 escapes while Ca^{2+} passes into solution, and hydration of the latter leads to very high alkalinity of the water. This is probably the way in which the hyperalkaline-water seeps formed near the modern Dead Sea Transform.

Field examination and mineralogical analyses show that Cr-bearing opaque minerals are unstable upon interaction with hyperalkaline solutions. The localization of ettringite with the highest Cr^{6+} concentrations in hydrothermal veins that cut CM rocks that are rich in opaque minerals (Fig. 2a) was a prompt for us to investigate possible formation mechanisms of Cr^{6+}-substituted ettringite at the expense of the Cr^{3+}, which originally entered the opaque minerals.

Only two constituents in the environment are known to oxidize Cr^{3+} to Cr^{6+}: dissolved oxygen and manganese dioxides. The oxidation of Cr^{3+} to Cr^{6+} by oxygen is relatively slow, requiring several months. Palmer and Puls (1994) monitored Cr^{6+} concentrations in batch tests using three different species of Cr^{3+}-contaminated rocks, including silty sand and silt. Over a 300 day period, they observed that Cr^{6+} concentrations became as large as 7 mg/L in one experiment, with the average soil Cr^{6+} concentration measuring about 10^{-2} mg/g soil. Since Mn is a minor constituent of the Nabi Musa rocks (Table 3), we infer that oxidation of Cr^{3+} occurred mostly by dissolved oxygen from hyperalkaline waters. Some Cr^{3+} may thus have oxidized to Cr^{6+} during the time in which Nabi Musa existed as an onshore mud volcano, in the Middle or Late Pleistocene (0.8–0.01 Ma) (Sokol et al. 2010).

Ettringite is worthy of special discussion, as it is a key phase for understanding the behavior of Cr in the mineral-forming system of the fossil mud volcano of Nabi Musa. The presence of relict primary CM mineral assemblages [namely, ye'elimite and different ferritic phases (Sokol et al. 2010)] indicates that the original compositions of some CM rocks were close to CSA clinker, in which CSHs and ettringite are the common hydration products (Chrysochoou and Dermatas 2006). The proportion of ettringites in the Nabi Musa rocks is low, and is largely controlled by the compositions of both the reacting sediment and the pore waters. Ettringite is primarily localized among retrograde products of high-Ca and low-Si metamorphic and among the Ca- and sulfate-rich, low-grade Hatrurim rocks. The calculated pH of pore water in equilibrium with typical low-grade Hatrurim rock is 12.3 (Table 9), or almost that of lime-saturated water (12.4). The phases that can crystallize at this pH are ettringite and hydrocalumite (Chrysochoou and Dermatas 2006), but no hydrocalumite has been found thus far in the Nabi Musa rocks. In the presence of excess SO_4^{2-} and Ca (indicated by the predominance of gypsum, calcium carbonates, and hydrosilicates in mineral assemblages), soluble alumina may have been the limiting factor for ettringite or hydrocalumite growth. Nabi Musa rocks are persistently low in Al (Table 3); the lowest Al:S ratios (from 0.5 to 0.2) are characteristic of rocks corresponding to the late hydrothermal stage. Inasmuch as no hydrocalumite can form at Al:S < 1, this phase, with its Cr^{6+} immobilization capacity higher than that of ettringite (Chrysochoou and Dermatas 2006), either never formed, or was fully replaced by ettringite, as the pH decreased to around 11 over time.

The occurrence of large Cr^{6+}-bearing ettringite crystals in veins, and its intergrowth with afwillite, indicates crystallization directly from solution, rather than a process of replacement of earlier hydrocalumite and a subsequent fall in pH to around 11. We have no irrefutable evidence of a primary origin for fine ettringite impregnated within both brucite veins and in the low-grade host rocks.

The relatively widespread distribution of ettringite within the MZ complexes and ettringite's ability to substitute both Cr^{3+} for octahedral Al^{3+} and CrO_4^{2-} for SO_4^{2-} in the channel positions (Poellmann et al. 1993; Perkins and Palmer 2000; Chrysochoou and Dermatas 2006) allow us to consider its behavior in prolonged

geological processes with regard to Cr immobilization.

Sulfate ettringite is stable over the widest range of pH (10.5–13) compared with other substituted ettringites (Chrysochoou and Dermatas 2006). As witnessed in the field, ettringite on weathered surfaces of MZ rocks is almost always fully replaced by finely aggregated aragonite, vaterite, calcite, and gypsum, but it commonly preserved inside the rocks. The Cr^{6+}-bearing species of ettringite did survive in Nabi Musa, and was discovered in the interior of the hill after removal of overburden. Hexavalent chromium-bearing ettringite could be retained because most of the rocks that make up the hill are low-permeablilty, natural analogs to cement. This is a system in which ettringite has the highest Cr^{6+} immobilization efficiency (Chrysochoou and Dermatas 2006). Natural ettringite never incorporates large amounts of Cr^{6+} (the highest CrO_4 content is 0.35 apfu, or SO_4:CrO_4 ~ 7.6), though, according to models, the equilibrium concentration of soluble Cr^{6+} reaches $2.73 \cdot 10^{-2}$ mol/kg H_2O (Table 9).

We suggest that chromatite formation in the MZ has been largely controlled by the peculiar climate conditions of the Judean Desert. In the winter season, subsequent to exposure during highway construction, the hill was penetrated with rainwater; the decrease in pore water alkalinity due to the presence of both CO_2 and H_2O led to the instability of newly exposed Cr^{6+}-bearing ettringite. The possibility of rapid dissolution of the oxyanion and its subsequent retention as CrO_4^{2-} in solution at pH near 9.5 (Table 8) was confirmed in leaching tests performed on samples of ettringite-bearing brucite veins. According to Chrysochoou and Dermatas (2006), both sulfate- and chromate-substituted ettringite decompose if the pH of pore solutions drops below 10.5.

In the studied rocks with Cr concentration below 420 ppm, many chromium minerals have not been identified. One can propose that some quantity of CrO_4^{2-} and $CaCrO_4^0$ species may incorporate onto solid phases, probably by sorption (Terai et al. 2006; Tang et al. 2007; Goh et al. 2008). In principle, the adsorbed species may have been another source of mobile Cr^{6+}, but we have not seen infallible proof of the presence of any other soluble CrO_4^{2-}-bearing compounds in the studied rocks. Thus, decomposition and dissolution of Cr^{6+}-containing solid phases, mainly Cr^{6+}-bearing ettringite, appears to be the most likely mechanism of Cr^{6+} release from the studied rocks.

With the onset of the hot season (May 2007), prolific chromatite precipitation began at the foot of Nabi Musa hill. According to field observations, mineralogical analyses, and thermodynamic modeling, there are two possible ways of chromatite formation. Chromatite may crystallize directly from supersaturated solutions on the evaporation barrier:

$$CaCrO_4^0 \leftrightarrow CaCrO_4 \quad (2)$$

Calcium chromate is characterized by inverse solubility; it becomes less soluble in water as the temperature increases: the solubility of $CaCrO_4$ per 100 g H_2O at pH = 7 is 2.25 g at 20 °C, 1.49 g at 40 °C, and as low as 0.83 g at 60 °C (Kirgintsev et al. 1972). Therefore, chromatite crystallization occurs preferentially during hot seasons. The solubility of calcium chromate dihydrate under ambient (*P*-*T*) conditions is 11 g per 100 g H_2O (Kirgintsev et al. 1972). Judging by the observed coexistence of the poorly crystalline phase $CaCrO_4 \cdot 2H_2O$ (Fig. 4a) with tiny precipitates of $CaCrO_4$, both crystallized simultaneously from pore waters that were supersaturated with respect to both phases.

The other possible chromatite formation mechanism is interaction between a solution enriched in a soluble Cr^{6+} species and calcium carbonate and/or gypsum (Eqs. 3 and 4):

$$CaCO_{3(s)} + CrO_4^{2-} \leftrightarrow CaCrO_4 + CO_3^{2-} \quad (3)$$

$$CaSO_4 \cdot 2H_2O_{(s)} + CrO_4^{2-} \rightarrow CaCrO_4 + SO_4^{2-} + 2H_2O \quad (4)$$

Reactions 3 and 4 are reversible, such that $CaCrO_4$ and most probably $CaCrO_4 \cdot 2H_2O$ dissolve during interaction of rocks with CO_2-bearing, meteoric waters, and Ca reprecipitates in the form of a calcium carbonate phase. It is not surprising that calcium carbonates and calcium chromates were observed both predating and postdating one another in the natural samples (Fig. 4).

Having failed to find a published diagram illustrating the chromatite stability field, we computed the Eh-pH diagram for a stoichiometric concentration of Cr (Fig. 10), which shows the stability fields of $CaCrO_4$, $Mg(OH)_2$, and Cr_2O_3. Thus, we can infer precipitation of $CaCrO_4$ from solutions that are anomalously rich in Cr^{6+} under extremely oxidizing conditions. The field of chromatite stability expands significantly as pH rises from 7 to 14, but is reduced if the activity of Ca is limited by the solubility of calcite (hatch lines on the diagram).

Concluding remarks

Field observations, analytical data on bulk chemistry, mineralogy, and leaching of rock samples from the Mottled Zone sequence, as well as thermodynamic modeling, have all provided clues to mechanisms that control the fate of Cr^{3+} and Cr^{6+} in particular geological environments, such as the Judean Desert. The exceptional scarcity of chromatite ($CaCrO_4$), discovered uniquely within two adjacent MZ localities of Maale

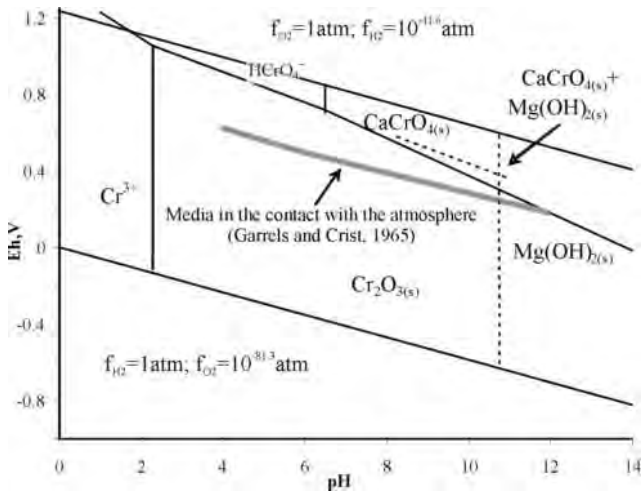

Figure 10. Eh-pH diagram of the system Cr-O-H-(Mg) at 298.15 K. Total chromium concentrations correspond to the stoichiometric dissolution of chromatite, i.e., $CaCrO_{4(s)} = [CrO_4^{2-}] \cdot [Ca^{2+}]$ from Wang and Li (2004). Dotted lines show the case when Ca concentration is limited by calcite solubility and Mg concentration is limited by the solubility of $Mg(OH)_{2(s)}$. Normal Eh-pH values measured in natural waters from Garrels and Christ (1965).

Adummim and Nabi Musa, is due to a set of physicochemical conditions that are unusual for natural, mineral-forming systems. They are, namely, (1) the primary Cr^{3+} accumulations in Ca-rich rocks; (2) interaction of the latter with hyperalkaline waters (pH ≥ 12) under surface oxic conditions that promote oxidation of Cr^{3+} to Cr^{6+}; (3) formation of Ca-H_2O-Cr^{6+}-bearing solid phases with the subsequent Cr^{6+} release into pore waters after dealkalization.

The arid climate of the Judean Desert is among the most important prerequisites for chromatite accumulation and short-term conservation. The store of Cr^{6+}-bearing ettringite remained buried until 2006 when it was exhumed during the construction of the Jerusalem-Jericho highway across the hill. With exposure to dry heating during summer seasons and to incongruent dissolution during rainy seasons, the mineral has experienced gradual decomposition. Decomposition and dissolution have been the key processes responsible for the release of Cr^{6+}, and Cr^{6+}-bearing ettringite appears to be the major source of Cr^{6+} for currently precipitated calcium chromate. Secondary immobilization of Ca within solid phases (calcite, aragonite, gypsum, and CSHs), has caused a continuous decrease of Ca content in the waters that drain the hill of Nabi Musa. On the other hand, the concentration of Cr^{6+} has grown, due to progressive decomposition of Cr^{6+}-bearing ettringite. As the amount of rain water that migrates downhill by capillary migration is very small, it gradually transforms into pore waters of high total salinity. Evaporation of pore water in the early summer of 2007 produced chromatite in the Nabi Musa area. Initially, calcium chromate arose because of the interaction of Cr^{6+}-rich water with calcite and gypsum. Then, gradual heating of air and rocks caused a rich precipitation of chromatite and $CaCrO_4 \cdot 2H_2O$ by direct capillary evaporation.

It is pertinent to note that the known natural occurrence of *water-soluble* potassium chromate (tarapacaite, K_2CrO_4), dichromate (lopezite, $K_2Cr_2O_7$), and calcium iodate-chromate [dietzeite, $(Ca_2(IO_3)_2(CrO_4) \cdot H_2O$] have been restricted thus far to the "incredible" Chilean nitrate deposits that contain a unique group of saline minerals, such as nitrates, iodates, borates, and perchlorates (Ericksen 1983). Although the climate of Judean Desert is milder than the extremely arid climate of the Chilean Atacama Desert, our mineralogical study of the Nabi Musa area promises that diverse rare species may be discovered among saline minerals. These would most likely include borates, because the Nabi Musa rocks are remarkably high in B, reaching concentrations of 200 ppm (Sokol et al. 2010).

ACKNOWLEDGMENTS

We thank associate editor Ian Swainson, and the anonymous referees whose thoughtful criticism inspired more insights and diversification in our analysis of the Mottled Zone Cr mineralization. We are grateful to E. Nigmatulina, N. Karmanov, I. Kupriyanov, and M. Khlestov (Sobolev Institute of Geology and Mineralogy, Novosibirsk, Russia) for the analytical work. More thanks go to A. Gilat (Geological Survey of Israel, Jerusalem) for valuable discussions. Thanks are extended to T. Perepelova, our translator, for improving and clarifying the English text. The study was supported by grants 09-05-00285 and 10-05-00518 from the Russian Foundation for Basic Research and grant MK-6750.2010.5 from the President of the Russian Federation.

REFERENCES CITED

Abed, A.M., Arouri, K.R., and Boreham, C.J. (2005) Source rock potential of the phosphorite-bituminous chalk-marl sequence in Jordan. Marine and Petroleum Geology, 22, 413–425.

Alexander, W.R. and Smellie, J.A.T. (1998) Maqarin natural analogue project: ANDRA, CEA, NAGRA, NIREX and SKB synthesis report on phases I, II and III. 101 p. Scientific Technical Report NPB 98-08. Nagra, Wettingen, Switzerland.

Bajda, T. (2005) Chromatite $CaCrO_4$ in soil polluted with electroplating effluents, Zabierzów, Poland. Science of the Total Environment, 336, 269–274.

Bentor, Y.K., Gross, S., and Heller, L. (1963) High-temperature minerals in non-metamorphosed sediments in Israel. Nature, 199, 478–479.

Bogoch, R., Gilat, A., Yoffe, O., and Ehrlich, S. (1999) Rare earth trace element distributions in the Mottled Zone complex, Israel. Israel Journal of Earth Sciences, 48, 225–234.

Burg, A., Kolodny, Ye., and Lyakhovsky, V. (1999) Hatrurim-2000: The "Mottled Zone" revisited, forty years later. Israel Journal of Earth Sciences, 48, 209–223.

Clark, I.D., Fritz, P., Seidlitz, H.K., Trimborn, P., Milodowski, T.E., Pearce, J.M., and Khoury, H.N. (1993) Recarbonation of metamorphosed marls, Jordan. Applied Geochemistry, 8, 473–481.

Clark, I.D., Dayal, R., and Khoury, H.N. (1994) The Maqarin (Jordan) natural analogue for ^{14}C attenuation in cementitious barriers. Waste Management, 14, 467–477.

Chrysochoou, M. and Dermatas, D. (2006) Evaluation of ettringite and hydrocalumite formation for heavy metal immobilization: Literature review and experimental study. Journal of Hazardous Materials, 136, 20–33.

Damidot, D. and Glasser, F.P. (1993) Thermodynamic Investigation of the CaO-Al_2O_3-$CaSO_4$-K_2O-H_2O System at 25 °C. Cement and Concrete Research, 23, 1195–1204.

Doyle, W.P., and Eddy, P. (1967) Infra-red of chromates (V) of calcium, strontium and barium. Spectrochimica Acta, 23A, 1903–1907.

Elie, M., Techer, I., Trotignon, L., Khoury, H., Salameh, E., Vandamme, D., Boulvais, P., and Fourcade, S. (2007) Cementation of kerogen-rich marls by alkaline fluids released during weathering of thermally metamorphosed marly sediments. Part II: Organic matter evolution, magnetic susceptibility and metals (Ti, Cr, Fe) at the Khushaym Matruk natural analogue (Central Jordan). Applied Geochemistry, 22, 1311–1328.

Ericksen, G.E. (1983) The Chilean nitrate deposits. American Scientist, 71, 366–374.

Fourcade, S., Trotignon, L., Boulvais, P., Techer, I., Elie, M., Vandamme, D., Salameh, E., and Khoury, H. (2007) Cementation of kerogen-rich marls by alkaline fluids released during weathering of thermally metamorphosed marly sediments. Part I: Isotopic (C, O) study of the Khushaym Matruk natural analogue (Central Jordan). Applied Geochemistry, 22, 1293–1310.

Gardosh, M., Kashai, E., Salhov, S., Shulman, H., and Tannenbaum, E. (1996) Hydrocarbon explosion in the southern Dead Sea area. In T.M. Niemi, Z. Ben-Avraham, and L. Gat, Eds., The Dead Sea: The lake and its setting, p. 57–72. Oxford Press, U.K.

Garrels, R.M. and Christ, C.L. (1965) Solutions, Minerals, and Equilibria, 450 p. Harper and Row, New York.

Gastaldi, D., Canonico, F., and Boccaleri, E. (2009) Ettringite and calcium sulfoaluminate cement: investigation of water content by near-infrared spectroscopy. Journal of Materials Science, 44, 5788–5794.

Geelhoed, J.S., Meeussen, J.C.L., Hillier, S., Lumsdon, D.G., Thomas, R.P., and Farmer, J.G. (2002) Identification and geochemical modeling of processes controlling leaching of Cr(VI) and other major elements from chromite ore processing residue. Geochimica et Cosmochimica Acta, 66, 3927–3942.

Gill, D. (1995) Geochemistry of the Arad basin phosphorites, southern Israel. Israel Journal of Earth Sciences, 44, 11–24.

Gilat, A. (1994) Tectonics and associated mineralization activity, Southern Judea, Israel, 280 p. Ph.D. thesis, Ministry of Energy and Infrastructure, Geological Survey of Israel, Mineral and Energy. Resources Division, Jerusalem (in Hebrew, English Abstract).

——— (1998) Hydrothermal activity and hydro-explosions as a cause of natural combustion and pyrolysis of bituminous rocks: The case of Pliocene metamorphism in Israel (Hatrurim Formation). Geological Survey of Israel, Current Research, 11, 96–102.

Goldreich, Y. (2003) The climate of Israel, observation, research and application, 270 p. Kluwer Academic/Prenum Publishers, New York.

Goh, K.-H., Lim, T.-Th., and Dong, Z. (2008) Application of layered double hydroxides for removal of oxyanions: A review. Water Research, 42, 1343–1368.

Grapes, R. (2006) Pyrometamorphism, 276 p. Springer, Berlin.

Gross, S. (1977) The mineralogy of the Hatrurim formation, Israel. Geological Survey of Israel, Bulletin, 80 p.

——— (1980) Bentorite. A new mineral from the Hatrurim area, west of the Dead Sea, Israel. Israel Journal of Earth Sciences, 29, 81–84.

Gvirtzman, H. and Stanislavsky, E. (2000) Palaehydrology of hydrocarbon maturation, migration and accumulation in the Dead Sea Rift. Basin Research, 12, 79–93.

Helgeson, H.C., Kirkham, D.H., and Flowers, G.H. (1981) Theoretical prediction of the thermodynamic behavior of aqueous electrolytes at high pressures and

temperatures: IV. Calculation of activity coefficients and apparent molal and standard and relative partial molal properties to 600°C and 5 kb. American Journal of Science, 281, 1249–1516.
Eckhardt, E.J. and Heimbach, W. (1963) Ein natürliches vorkommen von $CaCrO_4$, chromatite. Naturwissenschaften, 50, 612.
Jeffery, P.G. (1970) Chemical methods of rock analysis, 509 p. Pergamon Press, New York.
Kholodov, V.N. (1993) Types of sedimentary basin and feeder sources as a factors of matter differentiation. Lithology and Mineral Resources, 5, 3–26 (in Russian).
Khoury, H. and Nassir, S. (1982) High temperature mineralization in Maqarin area, North Jordan. Neues Jahrbuch für Mineralogie, Abhandlungen, 144, 197–213.
Kirgintsev, A.I., Trushnikova, L.N., and Lavrent'eva, V.G. (1972) Solubility of inorganic substances in water, 248 p. Chemistry, Leningrad (in Russian).
Kolodny, Y. (1979) Natural cement factory, a geological story. In J. Skalny, Ed., Cement production and use, p. 203–216. Conference Proceedings sponsored by the Engineering Foundation. U.S. Army Research Office, Ringe, New Hampshire.
Kopf, A.J. (2002) Significance of mud volcanism. Reviews of Geophysics, 40, 2, 1005.
Kulik, D.A. and Kersten, M. (2001) Aqueous solubility diagrams for cementitious waste stabilization systems: II, End-member stoichiometries of ideal calcium silicate hydrate solid solutions. Journal of the American Ceramic Society, 84, 3017–3026.
Larson, A.C. and Von Dreele, R.B. (2000) General Structure Analysis System (GSAS). Los Alamos National Laboratory Report LAUR, 86-748.
Macphee, D.E. and Barnett, S.J. (2004) Solution properties of solids in the ettringite- thaumasite solid solutions series. Cement and Concrete Research, 34, 1591–1598.
Matthews, A. and Gross, S. (1980) Petrologic evolution of the "Mottled Zone" (Hatrurim) metamorphic complex of Israel. Israel Journal of Earth Sciences, 29, 93–106.
Milodowski, A.E., Khoury, H.N., and Mäder, U. (2001) Mineralogical alteration by hyperalkaline groundwater in northern Jordan. In R. Cidu, Ed., Proceedings of the 10th Water-Rock Interaction Symposium in Villasimius, Italy, 2, 1347–1350. Balkema, Lisse.
Minster, T., Yoofe, O., and Nathan, Y. (1996) Geochemical database of oil shales from Israel. Geological Survey of Israel, Report TR-GSI/15/96.
Nakamoto, K. (1997) Infrared and Raman Spectra of Inorganic and Coordination Compounds, Part I: Theory and Applications in Inorganic Chemistry (Fifth edition), 383 p. Wiley, New York.
Nathan, Y., Shiloni, Y., Roded, R., Gal, I., and Deutsch, Y. (1979) The geochemistry of the northern Negev phosphorites (Southern Israel). Geological Survey of Israel, Bulletin, 73, 41 p.
Nikolaeva, I.V., Palesski, S.V., Kozmenko, O.A., and Anoshin, G.N. (2008) Analysis of geologic reference materials for REE and HFSE by inductively coupled plasma-mass-spectrometry (ICP-MS). Geochemistry International, 46, 1016–1023.
Palmer, C.D. (2000) Precipitates in a Cr(VI)-contaminated concrete. Environmental Science and Technology, 34, 4185–4192.
Palmer, C.D. and Puls, R.W. (1994) Natural attenuation of hexavalent chromium in groundwater and soil. EPA ground water issue no. EPA/540/5-94/505. U.S. Environmental Protection Agency, Oklahoma.
Perkins, R.B. and Palmer, C.D. (1999) Solubility of ettringite ($Ca_6[Al(OH)_6]_2(SO_4)_3 \cdot 26H_2O$) at 5–75°C. Geochimica et Cosmochimica Acta, 63, 1969–1980.
——— (2000) Solubility of $Ca_6[Al(OH)_6]_2(CrO_4)_3 \cdot 26H_2O$, the chromate analog of ettringite, 5–75°C. Applied Geochemistry, 15, 1203–1218.
——— (2001) Solubility of chromate hydrocalumite ($3CaO\text{-}Al_2O_3\text{-}CaCrO_4\text{-}nH_2O$) 5–75°C. Cement and Concrete Research, 31, 983–992.
Picard, L. (1931) Geological researches in the Judean Desert, 108 p. Goldberg Press, Jerusalem.
Piper, D.Z. (1994) Seawater as the source of minor elements in black shales, phosphorites and other sedimentary rocks. Chemical Geology, 114, 95–114.
——— (2001) Marine chemistry of the Permian Phosphoria Formation and basin, Southeast Idaho. Economic Geology, 96, 599–620.
Piper, D.Z. and Calvert, S.E. (2009) A marine biogeochemical perspective on black shale deposition. Earth Science Reviews, 95, 63–96.
Poellmann, H., Auer, St., Kuzel, H.J., and Wenda, R. (1993) Solid solution of ettringites. Cement and Concrete Research, 23, 422–430.
Rai, D., Zachara, J.M., Eary, L.E., Ainsworth, C.C., Amonette, J.E., Cowan, C.E., Szeimeczka, R.W., Resch, C.T., Schmidt, R.L., Smith, S.C., and Girvin, D.C. (1988) Chromium Reactions in Geologic Materials. Electric Power Institute Research no. EA-5741. Palo Alto, California.
Robie, R.A., Hemingway, B.S., and Fisher, J.R. (1978) Thermodynamic properties of minerals and related substances at 298.15 K and 1 Bar pressure and higher temperatures, 456 p. U.S. Geological Survey Bulletin no. 1452, U.S. Government Printing Office, Washington, D.C.
Sharygin, V.V., Sokol, E.V., and Vapnik, Ye. (2008) Minerals of the pseudobinary perovskite-brownmillerite series from combustion metamorphic larnite rocks of the Hatrurim Formation, Israel. Russian Geology and Geophysics, 49, 943–964.
Shvarov, Yu.V. (1999) Algorithmization of the numerical equilibrium modeling of geochemical processes. Geochemistry International, 6, 571–576.
Sokol, E.V. and Volkova, N.I. (2007) Combustion metamorphic events resulting from natural coal fires. In G.B. Stracher, Ed., GSA Reviews in Engineering Geology XVIII: Geology of Coal Fires: Case Studies from Around the World, 97-115. Geological Society of America, Boulder, Colorado.
Sokol, E., Novikov, I., Zateeva, S., Vapnik, Ye., Shagam, R., and Kozmenko, O. (2010) Combustion metamorphic rocks as indicators of fossil mud volcanism: New implications for the origin of the Mottled Zone, Dead Sea rift area. Basin Research, 22, 414–438.
Tang, Y., Elzinga, E.J., Lee, Y.J., and Reeder, R.J. (2007) Coprecipitation of chromate with calcite: Batch experiments and X-ray absorption spectroscopy. Geochimica et Cosmochimica Acta, 71, 1480–1493.
Techer, I., Khoury, H.N., Salameh, E., Rassineux, F., Claude, C., Clauer, N., Pagel, M., Lancelot, J., Hamelin, B., and Jacquot, E. (2006) Propagation of high-alkaline fluids in an argillaceous formation: Case study of the Khushaym Matruk natural analogue (Central Jordan). Journal of Geochemical Exploration, 90, 53–67.
Terai, T., Mikuni, A., Komatsu, R., and Ikeda, K. (2006) Synthesis of Cr(VI)-ettringite in portlandite suspensions as a function of pH. Journal of the Ceramic Society of Japan, 114, 299–302.
Vapnik, Ye., Sharygin, V., Sokol, E., and Shagam, R. (2007) Paralavas in a combustion metamorphic complex, Hatrurim Basin, Israel. In G.B. Stracher, Ed., GSA Reviews in Engineering Geology XVIII: Geology of Coal Fires: Case Studies from Around the World, 133–153. Geological Society of America, Boulder, Colorado.
Wang, T. and Li, Z. (2004) Some thermodynamic properties of calcium chromate. Journal of Chemical and Engineering Data, 49, 1300–1302.
Wazne, M., Jagupilla, S.Ch., Moon, D.H., Christos Christodoulatos, C., and Koutsospyros, A. (2008) Leaching Mechanisms of Cr(VI) from Chromite Ore Processing Residue. Journal of Environmental Quality, 37, 2125–2134.
Williams, W.J. (1979) Handbook of anion determination, 630 p. Butterworths, London
Yoffe, O., Nathan, Y., Wolfarth, A., Cohen, S., and Shoval, S. (2002) The chemistry and mineralogy of the Negev oil shale ashes. Fuel, 81, 101–117.

Manuscript received January 3, 2010
Manuscript accepted October 28, 2010
Manuscript handled by Ian Swainson